A global observational analysis to understand changes in air quality during exceptionally low anthropogenic emission conditions

Ranjeet Sokhi, Vikas Singh, Xavier Querol, Sandro Finardi, Admir Créso Targino, Maria de Fatima Andrade, Radenko Pavlovic, Rebecca Garland, Jordi Massagué, Shaofei Kong, et al.

A global observational analysis to understand changes in air quality during exceptionally low anthropogenic emission conditions

Ranjeet S. Sokhi [a,*], Vikas Singh [b], Xavier Querol [c], Sandro Finardi [d], Admir Créso Targino [e], Maria de Fatima Andrade [f], Radenko Pavlovic [g], Rebecca M. Garland [h,i,j], Jordi Massagué [c,k], Shaofei Kong [l], Alexander Baklanov [m], Lu Ren [n], Oksana Tarasova [m], Greg Carmichael [n], Vincent-Henri Peuch [o], Vrinda Anand [q], Graciela Arbilla [r], Kaitlin Badali [s], Gufran Beig [q], Luis Carlos Belalcazar [t], Andrea Bolignano [u], Peter Brimblecombe [v], Patricia Camacho [p], Alejandro Casallas [w,ae], Jean-Pierre Charland [s], Jason Choi [x], Eleftherios Chourdakis [y], Isabelle Coll [z], Marty Collins [aa], Josef Cyrys [ab], Cleyton Martins da Silva [ac], Alessandro Domenico Di Giosa [u], Anna Di Leo [ad], Camilo Ferro [ae], Mario Gavidia-Calderon [f], Amiya Gayen [af], Alexander Ginzburg [ah], Fabrice Godefroy [ai], Yuri Alexandra Gonzalez [t], Marco Guevara-Luna [aj], Sk. Mafizul Haque [af], Henno Havenga [i], Dennis Herod [al], Urmas Hõrrak [am], Tareq Hussein [an], Sergio Ibarra [f], Monica Jaimes [p], Marko Kaasik [am], Ravindra Khaiwal [ao], Jhoon Kim [ap], Anu Kousa [aq], Jaakko Kukkonen [ar,a], Markku Kulmala [an], Joel Kuula [ar], Nathalie La Violette [as], Guido Lanzani [ad], Xi Liu [l], Stephanie MacDougall [at], Patrick M. Manseau [g], Giada Marchegiani [u], Brian McDonald [au], Swasti Vardhan Mishra [af], Luisa T. Molina [ag], Dennis Mooibroek [av], Suman Mor [aw], Nicolas Moussiopoulos [y], Fabio Murena [ax], Jarkko V. Niemi [as], Steffen Noe [ay], Thiago Nogueira [f], Michael Norman [az], Juan Luis Pérez-Camaño [ba], Tuukka Petäjä [an], Stuart Piketh [i], Aditi Rathod [q], Ken Reid [bb], Armando Retama [bc], Olivia Rivera [p], Néstor Y. Rojas [t], Jhojan P. Rojas-Quincho [bd], Roberto San José [ba], Odón Sánchez [be], Rodrigo J. Seguel [bf], Salla Sillanpää [ar], Yushan Su [bg], Nigel Tapper [bh], Antonio Terrazas [p], Hilkka Timonen [ar], Domenico Toscano [ax], George Tsegas [y], Guus J.M. Velders [av], Christos Vlachokostas [y], Erika von Schneidemesser [bi], Rajasree VPM [a], Ravi Yadav [q], Rasa Zalakeviciute [bj], Miguel Zavala [ag]

[a] *Centre for Atmospheric and Climate Physics (CACP) and Centre for Climate Change Research (C3R), University of Hertfordshire, Hatfield, Hertfordshire, UK*
[b] *National Atmospheric Research Laboratory, Gadanki, AP, India*
[c] *Institute of Environmental Assessment and Water Research (IDAEA), Spanish Research Council (CSIC), Barcelona, Spain*
[d] *ARIANET, Milan, Italy*
[e] *Graduate Program in Environment Engineering, Federal University of Technology, Londrina, Brazil*
[f] *Departamento de Ciências Atmosféricas, Universidade de São Paulo, São Paulo, Brazil*
[g] *Meteorological Service of Canada, Environment and Climate Change Canada, Dorval, Canada*
[h] *Council for Scientific and Industrial Research, Pretoria, South Africa*
[i] *Unit for Environmental Sciences and Management, North-West University, Potchefstroom, South Africa*
[j] *Department of Geography, Geo-informatics and Meteorology, University of Pretoria, Pretoria, South Africa*
[k] *Department of Mining, Industrial and ICT Engineering, Universitat Politècnica de Catalunya, BarcelonaTech (UPC), Barcelona, Spain*
[l] *Department of Atmospheric Sciences, School of Environmental Studies, China University of Geosciences, Wuhan, China*
[m] *Science and Innovation Department, World Meteorological Organization (WMO), Geneva, Switzerland*
[n] *Center for Global and Regional Environmental Research, University of Iowa, Iowa City, United States*
[o] *ECMWF, European Centre for Medium-Range Weather Forecasts, Shinfield Park, Reading, UK*
[p] *Secretaria del Medio Ambiente de la Ciudad de México (SEDEMA), Mexico City, Mexico*
[q] *Indian Institute of Tropical Meteorology, Pune, Ministry of Earth Sciences, Govt. of India, India*

* Corresponding author.
E-mail address: r.s.sokhi@herts.ac.uk (R.S. Sokhi).

[r] *Universidade Federal do Rio de Janeiro, Rio de Janeiro, Brazil*
[s] *Analysis and Air Quality Section, Air Quality Research Division, Environment and Climate Change Canada, Ottawa, Canada*
[t] *Universidad Nacional de Colombia, Bogotá, Colombia*
[u] *Agenzia Regionale di Protezione dell'Ambiente del Lazio, Rome, Italy*
[v] *Department of Marine Environment and Engineering, National Sun Yat Sen University, Kaohsiung, Taiwan*
[w] *Earth System Physics, The Abdus Salam International Centre for Theoretical Physics (ICTP), Trieste, Italy*
[x] *Environment Protection Authority Victoria, Centre for Applied Sciences, Macleod, Australia*
[y] *Laboratory of Heat Transfer and Environmental Engineering, Aristotle University, Thessaloniki, Greece*
[z] *Université Paris-Est Créteil and Université de Paris, CNRS, LISA, Creteil, France*
[aa] *Air Monitoring Operations, Resource Stewardship Division, Environment and Parks, Edmonton, Canada*
[ab] *Institute of Epidemiology, Helmholtz Zentrum München, Neuherberg, Germany*
[ac] *Universidade Veiga de Almeida, Rio de Janeiro, Brazil*
[ad] *Agenzia Regionale di Protezione dell'Ambiente della Lombardia, Milano, Italy*
[ae] *Escuela de Ciencias Exactas e Ingenieria, Universidad Sergio Arboleda, Bogotá, Colombia*
[af] *Department of Geography, University of Calcutta, Kolkata, India*
[ag] *Molina Center for Energy and the Environment, CA, USA*
[ah] *A.M. Obukhov Institute of Atmospheric Physics, Moscow, Russia*
[ai] *Service de l'Environnement, Division du Contrôle des Rejets et Suivi Environnemental, Montréal, Canada*
[aj] *Conservación, Bioprospección y Desarrollo Sostenible, Universidad Nacional Abierta y a Distancia, Bogotá, Colombia*
[al] *National Smog Analysis, Analysis and Air Quality Section, Air Quality Research Division, Environment and Climate Change Canada, Ottawa, Canada*
[am] *Institute of Physics, University of Tartu, Tartu, Estonia*
[an] *Institute for Atmospheric and Earth System Research (INAR/Physics), University of Helsinki, Helsinki, Finland*
[ao] *Department of Community Medicine and School of Public Health, PGIMER, Chandigarh, India*
[ap] *Department of Atmospheric Sciences, Yonsei University, Seoul, South Korea*
[aq] *Helsinki Region Environmental Services Authority, Helsinki, Finland*
[ar] *Finnish Meteorological Institute, Helsinki, Finland*
[as] *Direction de la qualité de l'air et du climat, Direction générale du suivi de l'état de l'environnement, Ministère de l'Environnement et de la Lutte contre les changements climatiques Québec, Canada*
[at] *Air Quality Monitoring & Reporting, Nova Scotia Environment, Halifax, Canada*
[au] *National Oceanic and Atmospheric Administration, Chemical Sciences Laboratory, Boulder, USA*
[av] *National Institute for Public Health and the Environment (RIVM), Bilthoven, the Netherlands*
[aw] *Department of Environment Studies, Punjab University, Chandigarh, India*
[ax] *Department of Chemical, Material and Production Engineering (DICMAPI), Naples, Italy*
[ay] *Estonian University of Life Sciences, Tartu, Estonia*
[az] *Environment and Health Administration, City of Stockholm, Sweden*
[ba] *Computer Science School, ESMG, Technical University of Madrid (UPM), Madrid, Spain*
[bb] *Air Quality and Climate Change, Metro Vancouver Regional District, Burnaby, Canada*
[bc] *Independent Researcher, Mexico City, Mexico*
[bd] *National Meteorology and Hydrology Service, Lima, Peru*
[be] *Atmospheric Pollution Research Group, Universidad Nacional Tecnológica de Lima Sur, Lima, Peru*
[bf] *Center for Climate and Resilience Research (CR)2, Department of Geophysics, University of Chile, Santiago, Chile*
[bg] *Environmental Monitoring and Reporting Branch, Ontario Ministry of the Environment, Conservation and Parks, Toronto, Canada*
[bh] *School of Earth, Atmosphere and Environment, Monash University, Clayton, Australia*
[bi] *Institute for Advanced Sustainability Studies, Potsdam, Germany*
[bj] *Grupo de Biodiversidad, Medio Ambiente y Salud (BIOMAS), Universidad de Las Americas, Quito, Ecuador*

ARTICLE INFO

ABSTRACT

This global study, which has been coordinated by the World Meteorological Organization Global Atmospheric Watch (WMO/GAW) programme, aims to understand the behaviour of key air pollutant species during the COVID-19 pandemic period of exceptionally low emissions across the globe. We investigated the effects of the differences in both emissions and regional and local meteorology in 2020 compared with the period 2015–2019. By adopting a globally consistent approach, this comprehensive observational analysis focuses on changes in air quality in and around cities across the globe for the following air pollutants $PM_{2.5}$, PM_{10}, PMC (coarse fraction of PM), NO_2, SO_2, NOx, CO, O_3 and the total gaseous oxidant ($OX = NO_2 + O_3$) during the pre-lockdown, partial lockdown, full lockdown and two relaxation periods spanning from January to September 2020. The analysis is based on *in situ* ground-based air quality observations at over 540 traffic, background and rural stations, from 63 cities and covering 25 countries over seven geographical regions of the world. Anomalies in the air pollutant concentrations (increases or decreases during 2020 periods compared to equivalent 2015–2019 periods) were calculated and the possible effects of meteorological conditions were analysed by computing anomalies from ERA5 reanalyses and local observations for these periods. We observed a positive correlation between the reductions in NO_2 and NOx concentrations and peoples' mobility for most cities. A correlation between PMC and mobility changes was also seen for some Asian and South American cities. A clear signal was not observed for other pollutants, suggesting that sources besides vehicular emissions also substantially contributed to the change in air quality.

As a global and regional overview of the changes in ambient concentrations of key air quality species, we observed decreases of up to about 70% in mean NO_2 and between 30% and 40% in mean $PM_{2.5}$ concentrations over 2020 full lockdown compared to the same period in 2015–2019. However, $PM_{2.5}$ exhibited complex signals, even within the same region, with increases in some Spanish cities, attributed mainly to the long-range transport of African dust and/or biomass burning (corroborated with the analysis of NO_2/CO ratio). Some Chinese cities showed similar increases in $PM_{2.5}$ during the lockdown periods, but in this case, it was likely due to secondary PM formation. Changes in O_3 concentrations were highly heterogeneous, with no overall change or small increases (as in the case of Europe), and positive anomalies of 25% and 30% in East Asia and South America, respectively, with Colombia showing the largest positive anomaly of ~70%. The SO_2 anomalies were negative for 2020 compared to 2015–2019 (between ~25 to 60%) for all regions. For CO, negative anomalies were observed

for all regions with the largest decrease for South America of up to ~40%. The NO₂/CO ratio indicated that specific sites (such as those in Spanish cities) were affected by biomass burning plumes, which outweighed the NO_2 decrease due to the general reduction in mobility (ratio of ~60%). Analysis of the total oxidant (OX = NO_2 + O_3) showed that primary NO_2 emissions at urban locations were greater than the O_3 production, whereas at background sites, OX was mostly driven by the regional contributions rather than local NO_2 and O_3 concentrations. The present study clearly highlights the importance of meteorology and episodic contributions (e.g., from dust, domestic, agricultural biomass burning and crop fertilizing) when analysing air quality in and around cities even during large emissions reductions. There is still the need to better understand how the chemical responses of secondary pollutants to emission change under complex meteorological conditions, along with climate change and socio-economic drivers may affect future air quality. The implications for regional and global policies are also significant, as our study clearly indicates that $PM_{2.5}$ concentrations would not likely meet the World Health Organization guidelines in many parts of the world, despite the drastic reductions in mobility. Consequently, revisions of air quality regulation (e.g., the Gothenburg Protocol) with more ambitious targets that are specific to the different regions of the world may well be required.

1. Introduction

Drastic actions have been taken by governments across the world to limit movement and activities of populations to curtail the spread of the SARS-CoV-2 virus pandemic. Although the spread of COVID-19 (the disease caused by SARS-CoV-2) has had major health and socio-economic impacts across the globe, it has also presented an unique opportunity to understand how air quality in cities can change if large and rapid reductions in air pollutant emissions are implemented on regional and global scales. Through regional analysis, we can derive essential insights into how air quality changes have been driven by both meteorology and near instantaneous extreme reductions in anthropogenic emissions.

Many studies have reported on the reductions of emissions during the COVID-19 lockdown period. For example, Pomponi et al. (2020) used a macro-economic model combined with Google Community Reports to estimate reductions in air pollutant emissions for 129 countries due to restrictions on people's movement (i.e., mobility) within six categories: retail and recreation, groceries and pharmacies, parks, transit stations, workplaces and residential. Guevara et al. (2021) quantified the reductions in European primary air pollutant emissions for different sectors, such as energy, road traffic and aviation. Lapatinas (2020) examined mobility trends across Europe and showed that a combination of restrictive measures led to strong reductions in mobility during partial and full lockdowns. Despite the large number of studies reporting changes in air quality during lockdown periods, most have been limited to either a single or a relatively small number of cities, single country, single air pollutant or a specific region (e.g., Krecl et al., 2020; Singh et al., 2020; Grange et al., 2021; Shi et al., 2021).

A few regional or global studies are now emerging. Venter et al. (2020) reported on results using ground-based measurements of fine particulate matter ($PM_{2.5}$), nitrogen dioxide (NO_2) and ozone (O_3) taken from OpenAQ platform (https://openaq.org/) combined with satellite data. The study by Habibi et al. (2020) have also described changes in the same species based on data from the World Air Quality Index (WAQI, 2020) by comparing periods of 2020 with 2019. A similar approach, with the same data source and comparison of 2020 with 2019, has been followed by Kumari and Toshniwal (2020), which also included PM_{10} and sulphur dioxide (SO_2) and compared the changes in 12 cities. Using the same data source, He et al. (2021) have compared 2020 periods with 2015–2019 mean values on global and continental scales. Recently, Gkatzelis et al. (2021) have reviewed other published works and examined the results of studies about the effects of lockdowns on urban air pollution. They have emphasised the need for taking account of the effects of meteorology and atmospheric chemistry as well as emissions when assessing the changes in air quality due to lockdown measures.

It is evident, however, that there are only a few studies using primary data sources with consistent analyses to understand how the air quality changes have been affected by both the underlying meteorology and the drastic emission reductions within the context of seasonally driven

natural and anthropogenic air pollution events (such as dust storms, wildfires and other biogenic burning). It is only through such approaches that differences in pollutant concentration changes observed at different locations can be explained. Our methodological protocol, which is coordinated through the World Meteorological Organization Global Atmospheric Watch (WMO/GAW) programme, is aligned with the recommendations of many scientific organizations for reporting scientific results based on cohesive and consistent datasets (WMO, 2020).

In this study, we aim to examine changes in a wider set of air quality species and include the influence of meteorology on atmospheric oxidants which closely connect NO_2 and O_3. Specifically, we focus on explaining the changes in NO_2, oxides of nitrogen (NOx = NO + NO_2), particulate matter ($PM_{2.5}$, PM_{10}) and its coarse fraction (PMC = PM_{10} - $PM_{2.5}$), O_3, SO_2 and carbon monoxide (CO). We also examine the changes in NO_2/CO ratios to understand contributions from biomass burning and the changes in $PM_{2.5}$/PM_{10} ratios to evaluate contributions from the coarse and fine fractions of particulate matter. Our analysis spans 63 major cities in seven geographical regions of the world, viz., Australia, Europe, East Asia, North America, South Africa, South America and South Asia (Fig. 1). It should be noted that this study focuses on the changes in air quality due to the lockdown measures and not on how air quality or meteorology affects the spread of COVID-19 (WMO, 2021a).

To maintain a globally consistent analysis of several species, we have only used ground-based datasets supplied and checked by local data providers and do not attempt, for example, to incorporate satellite products. However, the readers are referred to other studies (e.g., Bauwens et al., 2020; Biswal et al., 2021), who have examined changes in NO_2 based on satellite datasets.

From an air pollution perspective, such an analysis should take account of a range of factors that are pollutant dependent. Emissions of air pollutants, such as CO and NOx, have continued to decline in many places regionally as a result of tighter emissions control in the industrial, vehicular and residential sectors (Zheng et al., 2019; McDuffie and Smith, 2020). In the case of $PM_{2.5}$ and PM_{10}, the emissions profile and chemical composition can vary from city to city across the globe (Philip et al., 2014; Karagulian et al., 2015; Cheng et al., 2016) depending upon contributions of the primary and secondary sources. The primary natural sources include windblown dust, crop/agricultural burning, volcanic ash, pollen particles and sea salt (van Donkelaar et al., 2016). Other natural emissions can also be a significant source of air pollution, for example sand and dust storms (SDS) and smoke from wildfires, which can make the interpretation of lockdown induced air quality changes more complex (e.g., Sessions et al., 2015; WMO, 2021b). On a global basis, secondary organic aerosol is mainly formed by the oxidation of biogenic volatile organic compounds (vegetation emissions of isoprene, monoterpenes, limonene, sesquiterpenes). With the transition to summertime in the Northern Hemisphere (NH), this pathway can also be a source of $PM_{2.5}$. Also, vegetation is a source of Primary Organic

Aerosol (Poschl and Shiraiwa, 2015).

On the other hand, key anthropogenic sources in a typical urban environment are exhaust and non-exhaust vehicular emissions, household, industrial and power plant emissions. Middle- and low-income countries rely on solid fuels for household cooking and heating, with the open burning of domestic waste being a common practice and contributing to the regional PM levels (Wiedinmyer et al., 2014). While the PM concentrations in Asian countries are among the highest, in many parts of the world they have started to decline (Zhai et al., 2019; Hammer et al., 2020; Singh et al., 2021).

In terms of highly reactive species, such as O_3 which are highly dependent on meteorological variables (e.g., Monks et al., 2015) and precursors (e.g., NOx and volatile organic compounds, VOCs), the changes in inter- and intra-annual meteorology can be as relevant as the reductions in emissions of precursors caused by lockdown policies (Ordóñez et al., 2020). Even with similar anthropogenic emissions of precursors, O_3 concentrations increase substantially from winter to summer seasons of the respective Northern and Southern Hemispheres due to enhanced photochemistry, increased availability of biogenic VOCs, evolution of the planetary boundary layer and enhanced regional and long-range transport (LRT) of pollutants (e.g., Millán, 2014). Similarly, as O_3 decreases from summer to winter, it is important to pinpoint whether the changes in O_3 concentrations observed from February (when pre-lockdown measures were implemented in many regions of the world) to July (relaxation period) were due to the usual - meteorologically driven mechanisms, the lockdown measures or a combination of both. As there is a high degree of uncertainty in VOC emissions and concentration data in many parts of the world (Gkatzelis et al., 2021), it was not included in the current analysis.

Daylight oxidant ($OX = O_3 + NO_2$) is a useful metric to shed light on how the atmospheric oxidation capacity changed during the COVID-19 pandemic in relation to local and regional O_3 contributions (Parker et al., 2020). The gaseous oxidant OX couples O_3 and NOx forming a closed cycle in which the interconversion of the NO-NO_2-O_3 triad yields no net chemical transformations during daylight hours (Clapp and Jenkin, 2001; Mazzeo et al., 2005) but preserves the total NOx and OX

mixing ratios. This mechanism makes OX less sensitive to specific local photochemistry and more influenced by the overall emission changes and photochemical oxidant production (Parker et al., 2020). Changes in OX can be interpreted as having a NOx-dependent contribution (due to local pollution, mostly primary NO_2) and a NOx-independent contribution (which roughly equates to the regional background O_3 concentrations). The approach disregards other processes that may change the O_3 mixing ratio, such as the downward entrainment of O_3-rich nocturnal residual layers, as it has been shown that O_3 is efficiently removed by titration overnight and by high dry deposition rates caused by turbulence (Hu et al., 2013).

Carbon monoxide concentrations in and around urban areas in the NH (e.g., US, Europe, and eastern Asia) are heavily determined by industrial and vehicular emissions (Zheng et al., 2019). In the Southern Hemisphere (SH), fires are a dominant source of CO pollution, especially in the tropics, although wildfires can also impact air quality over large areas in North America, Russia, and China (Holloway et al., 2000; Buchholz et al., 2018).

To understand the relative contributions from traffic and biomass burning, we use the NO_2/CO ratio, where high CO concentrations can be considered as a marker for biomass burning and NO_2 for road traffic, especially in urban traffic locations (Kalogridis et al., 2018). We used NO_2 as NO (and hence NOx) data were not available for several cities (including Chinese and South Korean cities, Naples, Quito and Lima).

From a meteorological perspective, we examine key variables that control atmospheric dispersion, removal and chemical processes, including air temperature, rainfall, wind speed and solar radiation (Oke et al., 2017). Indeed, Petetin et al. (2020), Dhaka et al. (2020), Le et al. (2020) and Kroll et al. (2020) have shown the dependence of NO_2, secondary $PM_{2.5}$ and O_3 concentrations on atmospheric variables during the COVID-19 lockdown. To distinguish between the changes induced by the reduction in anthropogenic emissions during the lockdown and those mediated by meteorology, we highlight the main meteorological features using both ground-based *in situ* measurement and ERA5 reanalysis datasets. We then examined whether reductions in local mobility were correlated with changes in air pollutants concentrations, such as
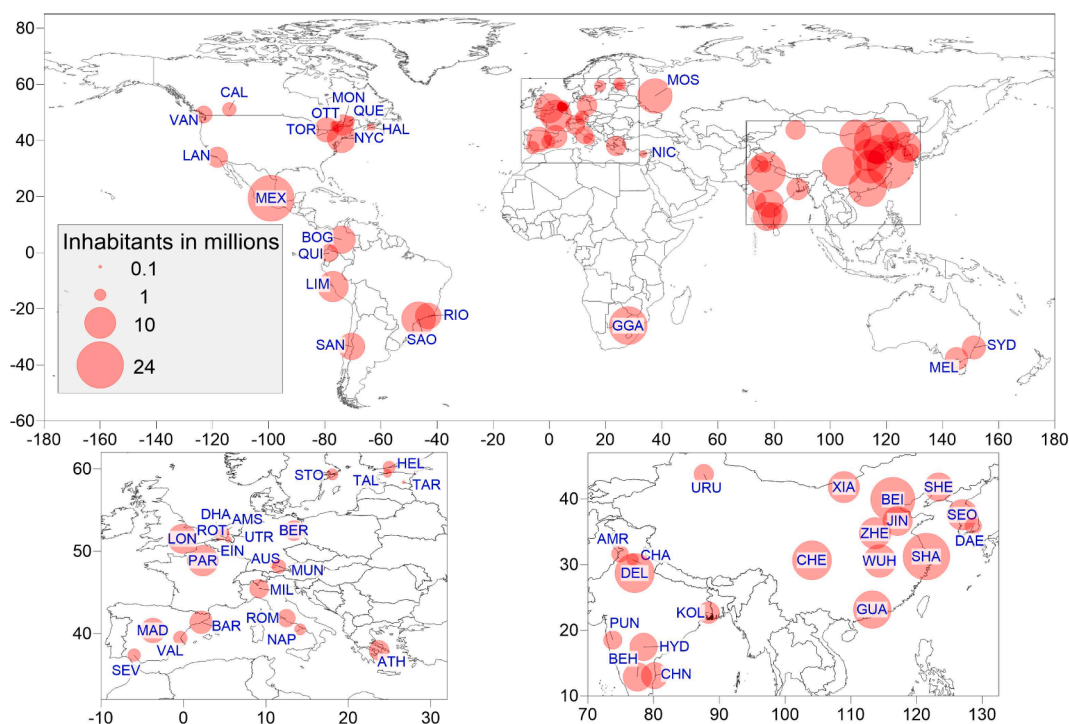

Fig. 1. Cities where the air quality impact of COVID-19 lockdown has been analysed. Circle size is proportional to the number of inhabitants. The cities acronyms are explained in Table S2.1.1.

those for NOx from the on-road vehicle fleet.

Such an analysis must be viewed in the context of ongoing emissions controls to improve air quality. For example, exhaust emission standards have led to general reductions in primary PM, NOx and SO_2 (e.g., EEA 2020). Sulphur dioxide has declined in many parts of the globe due to stricter emission controls and phasing out of coal. In China, for example, industrial coal boilers are major sources of SO_2 emissions (Zheng et al., 2018a; 2018b) although strengthening industrial emission standards, upgrades on industrial boilers and the phasing out of outdated industrial capacities is contributing to reductions since 2013 (Zhang et al., 2019). We assess whether the changes in air quality driven by the lockdown measures are representative of a scenario where drastic emission reductions would be sufficient to meet the World Health Organization (WHO) air quality guidelines. We also discuss if there are wider implications for relevant policies such as the Gothenburg Protocol.

2. Methodology

2.1. Description of cities and regions

This study examines data from 63 cities (See Supplementary Material Table S2.1.1) covering seven continental regions of the globe (Fig. 1). These cities represent regions with a range of environmental, climatic and socioeconomic conditions. While they are major global urban centres, they have different geographical and population sizes and represent different types of urban environments (Table S2.1.1), ranging from megacities (some exceeding 20 million inhabitants, such as Shanghai, São Paulo and Mexico City), to small cities (with roughly 0.1 million inhabitants, such as Tartu, Estonia). A wide range of climates is covered, from tropical to continental subarctic zones, with latitudes between 37.8° S (Melbourne) and 60° N (Helsinki) and elevations from sea level to 2800 m. Different conurbations are considered as the "inner" city and metropolitan areas. The socioeconomic metrics of per capita GDP span quite diverse conditions, from less than US$ 10,000 to more than US$ 80,000 (OECD, 2021; C40, 2021). The choice was also determined by the availability of quality-controlled air quality observations, participation of local data provider and the geographical coverage of the monitoring networks.

2.2. Defining lockdown periods for analysis

Lockdown periods varied from region to region. The specific dates were provided by the city data providers and validated with other data sources (e.g., OxCGRT, 2021). From this information, lockdown stages were defined to ensure a consistent comparison for the same city, across cities and regions. As the measures to limit movement and activities of people depended on rapidly evolving national and local responses to the pandemic spread, a small number of cities did not fall strictly into the definition of the lockdown phases presented below (e.g., Stockholm). For the purposes of the current analysis, the following periods were defined between January and September 2020:

Pre-lockdown: 30-day period before changes in mobility imposed by any lockdown measures.

Partial lockdown: period when some lockdown measures were introduced either only in part or on sub-national scale.

Full lockdown: period when full measures were introduced nationally.

Partial relaxation: period when lockdown measures were relaxed in part.

Full relaxation: period when lockdown measures were lifted to be closer to business as usual (BAU) conditions.

For the purposes of our analysis, we compare the changes in meteorology and air quality during the above lockdown periods for 2020 with the equivalent period means over 2015–2019 (BAU). By taking the equivalent lockdown periods of 2015–2019 to those of 2020, effects of seasonality are reduced. In the case of O_3, seasonality was taken into

account by comparing the observation data for the 'ozone' period of June and July for NH and September for SH.

In some cases, lockdown measures, while often stipulated and co-ordinated nationally, were implemented at a federal, state or city level. For this reason, the lockdown phases were checked to be consistent with local responses and cross checked with mobility changes, as shown in Fig. 2 for the cities considered in this study. Because different countries instituted the lockdown measures as the number of cases increased, the timings and strictness varied geographically, which led to a number of local specificities to be considered in the data analysis. For example, for cities located in the NH at extratropical latitudes, and for Santiago de Chile, the full lockdown occurred towards the end of the winter heating season (Table S2.1.1). Moreover, as southern Chinese cities are not usually equipped with centralised heating facilities, there were no changes in the usual situation during the lockdown. Seasonality differences and urban meteorology can also affect the air quality in and around cities and can add complexity to quantify the changes in air quality under the lockdown periods. While most of the responses to limit mobility during lockdown periods showed common features (as corroborated with the mobility data), the partial relaxation and full relaxation had different characteristics and timing as they depended on different responses by countries and cities. The full relaxation period should not be treated as strictly equivalent to the pre-pandemic BAU period, as economic activities had not returned fully to pre-pandemic levels.

2.3. Data sources and analysis protocols

2.3.1. Air quality data sources

In situ air pollutant data for the city stations were extracted from national or local operational air quality networks according to quality assurance and quality control (QA/QC) procedures (see Section 2.3.3). Data were analysed for 63 cities across the world encompassing 540 air quality monitoring stations. Table S2.3.1 provides the number of cities and stations for each lockdown period according to the air pollutant species of interest. While there was no city with a complete dataset for all pollutants, lockdown periods and site types, the most comprehensive datasets were for NO_2, O_3 and PM, with NO having the least coverage. The data were submitted in a prescribed format with means, median and standard deviations calculated from hourly values for each lockdown period of 2020 and for analogous periods of each year between 2015 and 2019 (referred to as BAU). PM_{10}, $PM_{2.5}$, NO, NO_2, CO, SO_2 and O_3 data were provided for different monitoring site types (traffic, urban, industrial and rural). In the case of O_3, the data were expressed as maximum daily 8-hour mean concentrations. The following *in situ* mean meteorological parameters were also used in the analysis: air temperature, relative humidity, global solar radiation, wind speed and precipitation. The changes in air pollutant concentrations and meteorological parameters were calculated as the difference between the mean value of each 2020 lockdown period and the mean value for the equivalent five-year BAU periods during 2015–2019. Percentage changes are given with respect to the equivalent 2015–2019 means.

The changes in the daylight OX mixing ratio (in ppb) were calculated for selected cities at traffic and background sites, by using paired hourly daylight (8:00–17:00) data. The analysis was performed by pooling the data for partial lockdown, full lockdown, partial and full relaxation periods of 2020, and the matching periods in the years from 2015 to 2019 (at some sites, from 2017 to 2019 due to lack of data). Linear regressions between the OX and NOx mixing ratios yielded the local (slope, α) and the regional (offset, β) contributions to OX (OX = NOx. α + β), following the approach outlined in Clapp and Jenkin (2001).

To examine possible effects of LRT of dust and smoke on the air quality in different regions of the globe during the lockdown periods, we used the data from the International Cooperative for Aerosol Prediction (ICAP) Multi-Model Ensemble (MME) Smoke and Dust Aerosol Depth Optical (AOD) forecasts (ICAP-MME, 2021; Sessions et al., 2015) and the

Fig. 2. Timing of COVID-19 lockdown measures in the different cities. (a) Lockdown period for different countries. (b) Mobility change in percentage.

WMO Sand and Dust Storms - Warning Advisory and Assessment System (WMO, 2021b).

2.3.2. Meteorological data

We used ERA5 meteorological reanalyses (Hersbach et al., 2020) to examine the impact of meteorological conditions on the air quality by computing global monthly mean anomalies of meteorological variables between the 2020 lockdown periods and their corresponding means in 2015–2019 (BAU). This BAU timeframe is considered long enough to include interannual meteorological variability, while not being affected significantly by influences from longer term climate phenomena or yearly anthropogenic emission variations (e.g., Le et al. (2020); Gama et al., 2021; He et al., 2021). ERA5 is the latest climate reanalyses produced by the European Centre for Medium-Range Weather Forecasts (ECMWF) and provides data on a regular latitude-longitude grid at $0.25° \times 0.25°$ resolution, suitable for regional scale analysis. We analysed meteorological anomalies from January to July 2020 covering most of the photochemical seasons in both hemispheres and including the lockdown, partial and full relaxation periods, when enhanced photochemistry favours O_3 production. During this period, available *in situ* meteorological observations were also used to validate the ERA5 anomalies.

2.3.3. Mobility data

Four databases were used to identify changes in mobility during the full lockdown period: Apple driving, Google retail, Waze and Baidu. The choice among these datasets was determined by the availability of information for each city. Most European and North American cities mobility data were based on Apple driving, while Baidu was used for China and Waze for South America. Google estimated the change in people's movement from 15 February 2020 onward based on Google Maps information on people's locations, such as at retail and recreation, grocery and pharmacy stores, parks, transit stations, workplaces, and residential places (https://www.google.com/covid19/mobility/). The changes were estimated with reference to the baseline days that represent a normal value for that day of the week. The baseline day is the median value from the five-week period between 3 January and 6 February 2020.

The Apple mobility data is from smart devices, considering the change from baseline, that is the volume on 13 January 2020 (http://covid19.apple.com/mobility).

For Waze, the data were the driven kilometres (or miles) percent change related to the baseline (http://www.waze.com/covid19) taken as the average value for the corresponding day of the week in the period February 11 to 25, 2020. Baidu mobility data consisted of the migration index available at http://qianxi.baidu.com/. Baidu gathers location data based on GPS, Wi-Fi and IP addresses of internet devices (China data lab, 2020). Mobility data for some cities (e.g., Urumqi and Nicosia) were not available for any of the periods.

The Supplementary Material (Figure S2.3.1) presents a comparison of the mobility data provided by these different databases and the agreement of their responses during the lockdown period in each city. It can also be observed that the mobility recorded during the full relaxation phase had not returned to the same level as the pre-lockdown

period. It seemed that there was no return to the "normal" configuration in terms of mobility after relaxation (Figure S2.3.2).

2.3.4. Data quality control protocols

While we used air quality data extracted from official sources, in some cases for 2020, the data may not have undergone the final quality assurance and quality control steps. Each step of the data provision, however, was checked and verified before conducting our analyses. This was ensured firstly by the data providers and subsequently by the core analysis team. In almost all cases, data were only used from official network stations with at least 70% of coverage of quality-controlled data for each period. Most of the sites had over 90% available data, but there were few cases when the availability threshold was lowered to 60%, where it was particularly difficult to obtain data from alternative official sources. Similarly, in a few cases where coverage was less than five previous years (e.g., Moscow, Augsburg and Munich), data for the two previous years were accepted. Standard data checks were also applied, such as consistency in units, formatting, naming criteria and leap year timing.

3. Results analysis and discussion

3.1. Changes in mobility and emissions

Vehicular emissions were one of the most affected anthropogenic air pollution sources, as a result of mobility restriction during the lockdown (Guevara et al., 2021; Biswal et al., 2021). However, changes in mobility varied largely across cities and lockdown phases, with the greatest reductions observed during the full lockdown (Fig. 2b). Reduction in mobility exceeded 70% in many cities across the globe during full lockdown, such as Greater Gauteng, the Chinese cities of Wuhan, Xi'an, Zhengzhou, all the Indian cities, in Europe (Paris, Naples, Milan and Rome) and in South America (Bogotá, Quito and Lima). While the reductions were smaller than 50% for other cities (Guangzhou, Daegu, Helsinki, Rotterdam, Den Haag, Halifax, Calgary, Los Angeles, New York, Moscow, Melbourne and Sydney). All Spanish cities reported mobility reductions above 65% even during the partial relaxation period.

To assess the linkages between mobility and air pollutant concentrations, the mean reduction in mobility during the full lockdown was correlated with the reduction in the pollutant concentrations. In the regression model, the R^2 is presented together with the 95% Confidence Intervals for the slope and intercept in the linear fit. Fig. 3 shows a clear positive correlation for cities with R^2 of 0.513 (p = 0.000) for NOx (excluding Helsinki site as it had a ratio outside the average of the distribution). Helsinki was considered an outlier because it deviates markedly from the behavior of the other sites, especially from the European cities. Including Helsinki, the slope of the linear regression changed by more than 16%, and the R^2 was 0.381.

Some cities showed a smaller decrease (less than 30%) in both NO and NOx concentrations during the lockdown (Kolkata, Ottawa and Toronto), despite the restrictions in mobility, indicating that other sources (e.g., energy generation and biomass burning emissions) could have had a substantial influence on NOx ambient concentrations. In Europe, except for Helsinki, the reduction in NOx was strongly correlated to the change in mobility. For example, cities in Spain (Madrid, Seville, and Barcelona) experienced a decrease of 80% in mobility and 60% in NOx during full lockdown. Venter et al. (2020), analysing data from different countries, found the same strong association between NO_2 and mobility reductions, discussing the importance of reducing the transport activity to reach NO_2 values near the air quality guidelines. They did not find significant associations between mobility reduction and $PM_{2.5}$ anomalies.

The figures in the Supplementary Material (S3.1.1 to S3.1.6) present the linear regression and the 95% confidence interval between the change in mobility and the change in CO, $PM_{2.5}$, NO_2, PMC
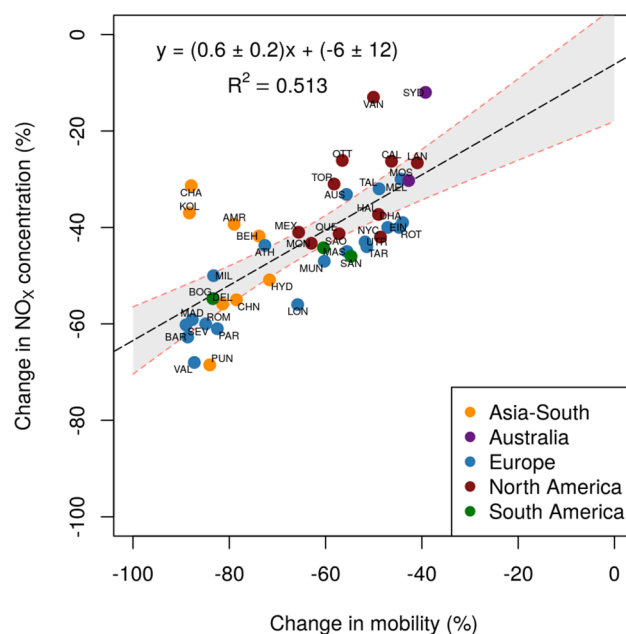

Fig. 3. Relationship between the reduction in NO_x concentrations and the reduction in mobility in the studied cities (except for Helsinki) during the full lockdown period. The data points are coloured according to regions. The shaded area represents the 95% Confidence Interval.

concentrations for all station types and PMC for transit stations for Indian, Chinese (Figure S3.1.5) and South American cities (Figure S3.1.6) during the lockdown. Of these air pollutants, NO_2 had the strongest correlation (R^2 = 0.343, p = 0.000), while the changes in $PM_{2.5}$ and CO concentrations did not correlate with the changes in mobility. In the case of $PM_{2.5}$, this can be partly attributed to atmospheric chemical reactions that favour the formation of secondary aerosols (e.g., Kroll et al., 2020). The clear correlation between changes in mobility and NO_2 concentrations can be attributed to its rapid formation through oxidation of NO by O_3 especially near road traffic locations.

The scatter in the data between mobility and air pollutant changes is most likely due to meteorological variabilities, possible contribution from other sources and differences in fleet compositions in the cities (e.g., diesel/gasoline/CNG and private/public/freight compositions). Our findings, however, are consistent with the study by Guevara et al. (2021) who estimated a mean reduction of 33% in NOx emissions, of which 85% was attributable to road transport in Europe. Habibi et al. (2020) also reported changes in mobility trends during lockdowns but considered monthly means instead of the regulated specific lockdown periods.

In the case of CO, confounding factors, such as the burning of wood for heating that increased during winter/early spring and the impact of agricultural biomass burning, may have interfered with the correlations (see Figure S3.1.1). A large body of observational studies has reported the use of solid fuel for heating in European households with direct impacts on the air quality (e.g., Caseiro et al., 2009; Maenhaut et al., 2012; Fuller et al., 2014; Kukkonen et al., 2020). For the Asian cities, positive but nonsignificant correlations between change in mobility and PMC concentration at traffic stations were observed (with R^2 of 0.595 and 0.294, for China and India, respectively, Figure S3.1.5). Although we only have PMC data for four South American cities, the high correlation (R^2 = 0.905) agrees with the estimates of emission inventories that associate the resuspension of road dust with vehicular movement (see Figure S3.1.6).

3.2. Implications of prevailing meteorology to changes in air quality

Although this study extends from January to September 2020, for the sake of brevity, we present here the analyses for the months of February

(full lockdown in China and pre-lockdown elsewhere), April (full lockdown in most countries) and June (partial or full relaxation in most countries), as they cover the most important lockdown periods and the photochemically active period in the NH and partially in the SH (Cooper et al. 2014). Fig. 4 shows ERA5 reanalysis-derived anomalies for April 2020 compared to 2015–2019, while mean observed *in situ* anomalies for the lockdown periods defined in Section 2.2 are illustrated in Figure S3.2.8. Detailed analysis of the prevailing meteorology is supported by Figures in Section S3.2.

A warm anomaly was recorded globally (NCEI/NOOA, 2020) in February 2020 with respect to the 1981–2010 Normals, with particularly strong intensity over Eurasia and Canada, persisting even when compared to the period 2015–2019 (Figure S3.2.2). The expected reduction in residential heating emissions and the increase in rainfall over southern China could have led to improved air quality in the region during this period. In northern China, on the other hand, the increase in humidity but unchanged precipitation and calm winds may have worsened the air quality. Over continental Europe, favourable dispersion conditions occurred in February 2020 with warmer temperatures and increase in wind speed, precipitation, and boundary layer depth (BLD). Sub-regional differences were observed, with the western and central Mediterranean recording drier conditions and lower wind speed. Warm and dry anomalies with respect to 2015–2019 were observed in Russia, Canada and in the northeastern US, while in other regions the anomalies were negative or modest with weaker wind speeds and reduced BLD. Southeastern Australia was colder, wetter and more overcast during this month in 2020.

For April 2020, the meteorological influence on the air quality was heterogeneous over the regions, being positive where precipitation and wind speeds increased and negative where lower wind speed and drier conditions occurred. Globally, a positive temperature anomaly for April 2020 with respect to the 1981–2010 Normals (NCEI/NOOA, 2020) was observed, but it was weaker than in February. Heterogeneities were apparent in many regions. For example, temperatures were higher in the 2020 lockdown periods compared to 2015–2019 in eastern Russia and central Asia, while they were lower in India, China, southeastern Africa and southeastern Australia (Figures 4 and S3.2.8). While there were pronounced large-scale rainfall and solar radiation anomalies, China was drier and received up to 40 W/m^2 more solar radiation during April 2020 than in the equivalent period in 2015–2019 (Figure S3.2.4). Southeastern Australia, Bay of Bengal and southeastern Africa, on the other hand, were wetter, with reduced solar radiation and BLD (Figure

S3.2.4). Temperature and rainfall variations were less noticeable in central and southern South America, but the Intertropical Convergence Zone intensified and became more organised. North America was colder and drier, while Mexico was warmer, without substantial differences in humidity and precipitation during April 2020 relative to 2015–2019. Fair weather and a warmer period generally dominated the whole month over continental Europe (van Heerwaarden et al., 2021), including the British Isles, Sweden and the northern Mediterranean with increased solar radiation and reduced rainfall. A cold anomaly was detected over the Mediterranean Area and eastern Europe, including Moscow, with increased precipitation over the Iberian Peninsula and southern Balkans (Fig. 4). March and April 2020 anomalies with respect to 2015–2019 (Figures S.3.2.3-S3.2.4) caused the variability in local meteorological observations (Figure S3.2.8a) in the European cities during the full lockdown.

Although June 2020 was ranked as the third warmest month on record (NCEI/NOOA, 2020), its temperature anomalies were weak or negative when compared to 2015–2019 period (Figure S3.2.6). Moreover, decreased solar radiation and increased humidity and precipitation led to unfavourable conditions for O$_3$ production everywhere, apart from Scandinavia and eastern Canada. Negative pressure anomalies occurred over Europe, western North America, southern South America and central Asia, during June 2020, while positive ones were detected in Scandinavia and eastern Canada (Figure S3.2.6). Northern India and eastern Brazil along with Europe, western North America, Chile and northern Asia, showed lower temperatures and increased humidity (Figure S3.2.6). An increase in precipitation was detected over northeastern India, eastern China and Korea, southern Brazil, Chile, Italy and eastern continental Europe, which would contribute to lowering air pollutant concentrations. Summer months anomalies cannot be easily superposed with partial and full relaxation periods due to their quite different time span in the studied locations (Fig. 2a).

Out of the monthly analysis, the most relevant features recorded during January–July 2020 with respect to 2015–2019 have been: a) the positive temperature anomaly affecting Eurasia and eastern North America from January to March; b) the prevailing cold and humid anomalies over northern India from February to June; c) the cold and dry conditions over western Canada during March and April; d) the cold and wet anomalies affecting continental and Mediterranean Europe during June and July.
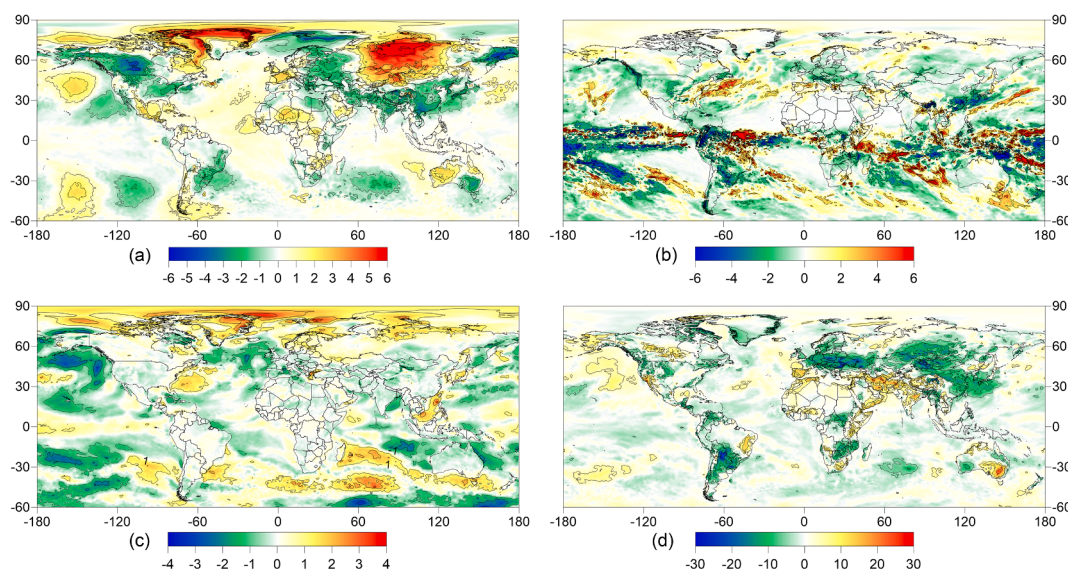

Fig. 4. April 2020 anomalies with respect to 2015–2019 mean ERA5 reanalysis of (a) 2-m temperature (K), (b) precipitation rate (mm/day), (c) 10-m wind-speed (m/s), (d) 2-m relative humidity (%).

3.3. Air quality and long-range transport of pollutants

Air pollution episodes are usually associated with anticyclonic conditions (Holzworth, 1969), particularly with lingering and slow-moving high-pressure systems (Wang and Angell, 1999; Zhu et al., 2018). The monthly pressure anomalies at both sea level pressure (SLP) and 500 hPa were positive over parts of China, Europe and North America in February (Figure S3.2.2) and over parts of Europe, Asia and North America in March and April (Figures S3.2.3–S3.2.4), potentially affecting the air quality during pre- to full-lockdown periods. However, Vancouver was the most affected city included in this study with persistent SLP and 500 hPa positive anomalies in February, March and April (Figures S3.2.2–S3.2.4). The evolution of pressure systems during the lockdown period forced the LRT paths of smoke from biomass burning and desert dust. Based on the daily ICAP/MME smoke AOD forecast averages (see Section 2.3.1), we observed that numerous Asian and South American cities were exposed to smoke pollution during their lockdown periods. Smoke has been reported to affect these regions during this time of the year, perhaps with the only exception for northern South America, which experienced persistent, higher-than-normal smoke events during lockdown periods, particularly in Bogotá (ICAP-MME, 2021; Mendez-Espinosa et al., 2021; INPE, 2021). There were a few cases in which smoke events occurred just outside the period examined in this investigation but did not affect our analysis (e.g., for Sydney and Melbourne, see Brimblecombe and Lai, 2021).

Data from the WMO SDS-WAS Regional Centre in Barcelona (WMO, 2021b) have shown that the monthly mean dust concentrations (originating from North Africa and the Middle East) for March, April and May 2020 in parts of Spain, Italy, Germany and the Balkans were between 5 and 20 $\mu g/m^3$. However, the same regions were affected by SDS events, raising the dust concentrations to between 50 and 200 $\mu g/m^3$. Comparing 2020 data with monthly mean dust concentrations estimated by the same source (WMO, 2021b) for the years 2015–2019, the dust load over Europe during the lockdown appears to be within the inter-annual variability. Data from other Regional Centres hosted by China have shown that major SDS storms affected several Chinese cities between February and May 2020, which is also in agreement with ICAP/MME dust AOD forecasts (Figures S3.3.1–S3.3.6). Table S3.3.1 lists the cities affected by these events and the possible impact on $PM_{2.5}$ concentrations, which are examined further in Section 3.4.

The El Niño-Southern Oscillation (ENSO) could have an impact on emission changes, in particular on wildfire induced emissions, by triggering specific spatial and temporal variations in forest fire potential (Inness et al., 2015; Zhao et al., 2018; Fang et al., 2021). The targeted analysis period of January–June 2020, however, did not show a strong ENSO signal according to the NOAA Oceanic Niño Index (NOAA, 2021). On the other hand, the reference period (2015–2019) was characterised by mixed ENSO signals with warm, cold or near-neutral phases. Based on these observations, no relevant ENSO-related wildfire emission anomalies were expected for the cities considered in 2020. Moreover, the analysis period does not include the months in which ENSO's impacts on emissions are the greatest, with the sole exception of January and February in southern China (Zhao et al., 2018; Sun et al., 2018).

To address volcano-related SO_2 pollution, we analyzed historical volcanic eruption data from NOAA's Global Sulfur Dioxide Monitoring (https://so2.gsfc.nasa.gov/). Based on these satellite observations, there were no major volcanic eruptions in the proximity of the analysed cities during the 2020 period of interest. During 2015–2019, the eruption of a volcano in Kamchatka (Russia) in June 2019 affected parts of the Arctic, Alaska and Canada, and the eruption of volcano Calbuco (Chile) in April 2015 affected parts of Chile, Brazil, and Argentina, including Buenos Aires.

3.4. Changes in air pollutant concentrations during the lockdown periods

The following sections discuss the anomalies for each of the air pollutants, supported by Fig. 5 and Figures S3.4.1–S3.4.26 showing the percentage anomalies for 2020 lockdown periods compared to mean of BAU 2015–2019 period. For each of the air pollutants we first consider the changes over the equivalent periods during BAU, then the changes during the lockdown period in 2020 and we finally discuss the changes according to the type of environment indicated by the type of sampling sites. In the case of CO and SO_2, we only present here a discussion of the results during 2020 for the sake of brevity.

3.4.1. Particulate matter

(i) Particulate matter concentrations for 2015–2019

Globally, $PM_{2.5}$ concentrations showed large spatial variations during BAU, ranging from as low as 5 $\mu g/m^3$ in Canada to over 150 $\mu g/m^3$ in China (Figure S3.4.1a). Chinese and Indian cities recorded higher concentration than other cities (within the range of about 50–160 $\mu g/m^3$), followed by cities in South Korea, Colombia and Chile (20–40 $\mu g/m^3$). The European cities recorded concentrations of 10–15 $\mu g/m^3$ (except for Milan), with the lowest concentrations (below 10 $\mu g/m^3$) in the north European cities, Australia and Canada. Inter-annual variations of up to ~50% in $PM_{2.5}$ were observed during 2015–2019 (Figure S3.4.1a). The concentrations were lower for most of the cities during 2018–2019 as compared to 2015–2016, however a clear trend has not been observed, as also reported by other studies which showed a decline in $PM_{2.5}$ over recent years (Zhai et al., 2019; Hammer et al., 2020; Singh et al., 2021). It could be due to the shorter data averaging period (lockdown periods) considered in this study as compared to monthly means used over several years by those studies. The BAU means for different lockdown periods shown in Figure S3.4.1b exhibited a strong seasonal pattern. The concentrations decreased from the equivalent pre-lockdown to full relaxation periods because of the transition from winter to summer in the NH and increased in Australia and South America because of the transition from summer to winter. These seasonal variations in $PM_{2.5}$ were driven mainly by changes in meteorological conditions (e.g., wintertime thermal inversions) and increase in local heating emissions during the transition from winter to summer and vice-versa (Cheng et al., 2016).

(ii) Relative changes in $PM_{2.5}$ concentrations for 2020 compared to 2015–2019

Most cities recorded lower $PM_{2.5}$ concentrations (Figure S3.4.1c) and negative percentage changes (Fig. 5a, S3.4.1d and S3.4.2) during lockdown periods as compared to BAU. Despite the lack of restriction in mobility, a reduction of over 50% was observed during pre-lockdown in London, Paris, Augsburg, Munich, Stockholm, and all over the Netherlands. These reductions were associated with the favourable meteorological conditions over Europe, namely higher wind speeds, precipitation rate and BLD (see Section 3.2 and Figures S3.2.1–S3.2.2). Reductions in $PM_{2.5}$ concentrations were observed across all the cities during the partial lockdown, except for an unusual increase of 71% in Vancouver (Figures 5 and S3.4.2) associated with persistent anticyclonic conditions, low wind speeds and poor dispersion. Because China did not enforce any partial lockdown, a specific analysis for this period was not possible. For India, a noticeable reduction was observed during the partial lockdown despite lesser restrictions on mobility (Singh et al., 2020).

During the full lockdown, reductions in $PM_{2.5}$ concentrations were observed in both NH and SH cities, more notably in India, a few Chinese cities (Chengdu, Guangzhou, Wuhan), Tartu, Seville, Moscow, Montreal, Mexico City, Quito and Lima. Conversely, the $PM_{2.5}$ concentrations increased in Beijing, Shenyang, Xi'an, Madrid and Valencia. However, in many European cities, the reductions were far less than observed in many other cities globally. Smaller reductions or even an increase over Chinese and European cities were associated with contributions due to meteorological transport and non-linear processes (e.g., inhibition of particulate matter dispersion due to low wind speed and BLD, and secondary PM formation favoured by increase in RH, Wang et al., 2020b; Le et al., 2020). In addition, for cities in northwestern Europe (e.g., Paris,
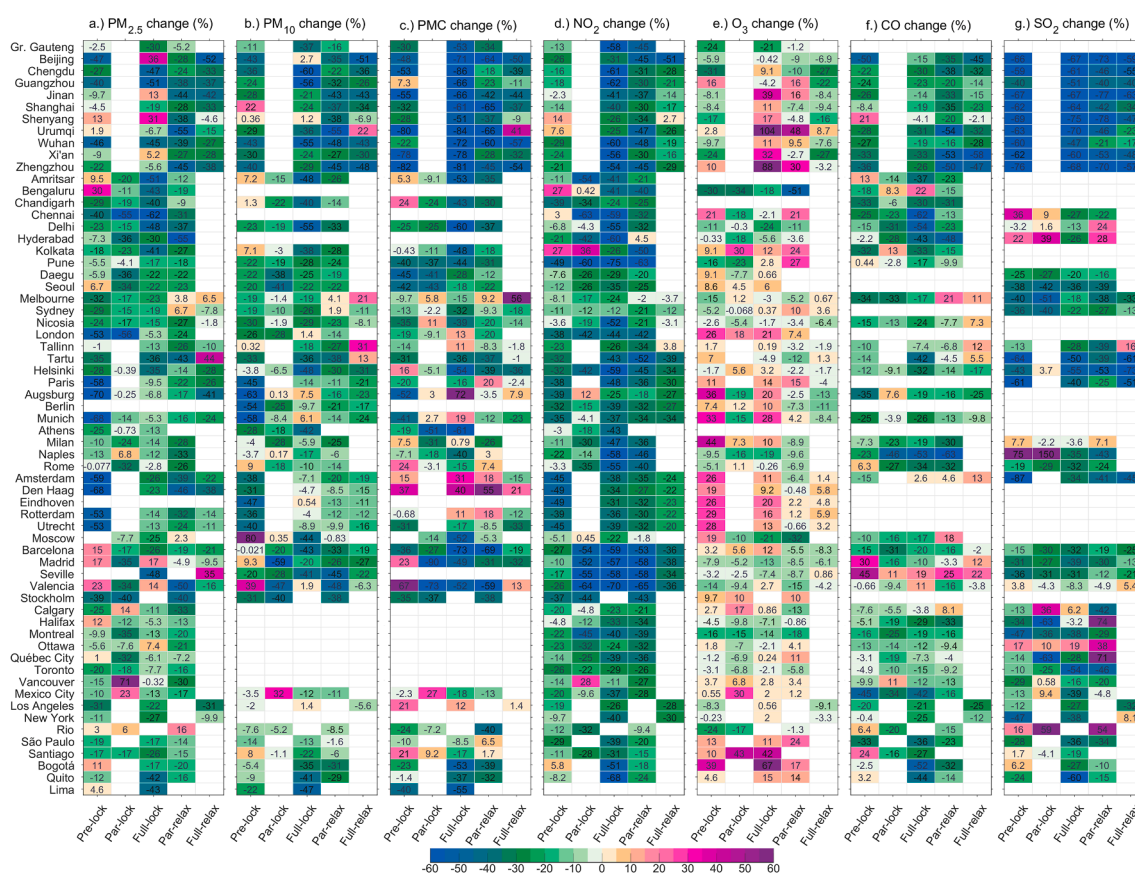
Fig. 5. Observed percentage changes for (a) PM$_{2.5}$, (b) PM$_{10}$, (c) PMC, (d) NO$_2$, (e) O$_3$, (f) CO, (g) SO$_2$ for the lockdown periods in 2020 compared to their corresponding periods in 2015–2019. The mean concentrations for different lockdown periods during BAU (2015–2019) and 2020 along with global maps of percentage changes are shown in the supplementary Figures from S3.4.1 to S3.4.26.

London and Dutch cities), the lesser reductions in PM$_{2.5}$ could be associated with formation of secondary inorganic aerosols associated with increased ammonia emissions during the spring season (Backes et al., 2016) and also the formation of secondary organic aerosol from the biogenic VOC emissions (Poschl and Shiraiwa, 2015; Kroll et al., 2020).

The lower-than-expected reductions over extratropical cities (e.g., European, Canadian cities) during the full lockdown (early spring) could be due to the enhancement of residential heating. Estimates for North America and Europe (EEA, 2020; Menut et al., 2020) indicated that residential wood combustion emissions increased by about 20% as more people were at home. This suggests that the lockdown measures led to increases in PM$_{2.5}$ emissions (e.g., residential wood combustion) in March and April in the NH, outweighing the PM$_{2.5}$ decreases from other sources (e.g., road traffic). For instance, in many Nordic cities, residential wood combustion is one of the two most important urban sources of PM$_{2.5}$ pollution, in addition to vehicular traffic (Kukkonen et al., 2018). In the case of Spanish cities, Querol et al. (2021) also have reported smaller decreases in PM$_{2.5}$ (with a few exceptions of increases), which they attributed to secondary aerosol formation driven by favoured meteorological conditions and, in some cases, due to incremental contributions from domestic and agricultural biomass burning. For the SH cities, residential wood burning for heating could have also increased in during SH winter months (eg. Morales-Solís et al., 2021) that could have impacted the net reduction in PM$_{2.5}$ emission during the lockdown phases.

Despite the lift of some restrictions during the partial relaxation phase, reductions of up to 55% were observed, except for the Australian cities, Moscow, and Rio de Janeiro. The European, Canadian and Chinese cities observed larger reductions during the partial relaxation than during full lockdown (typically 15–25% in Europe and Canada; and

25–55% in China). Most of the cities continued to show reductions during full relaxation, except for Melbourne, Tartu and Seville.

(iii) Relative changes in PM$_{10}$ and PMC concentrations for 2020 compared to 2015–2019

Like PM$_{2.5}$, most cities recorded lower PM$_{10}$ and PMC concentrations during all lockdown periods as compared to BAU (Fig. 5b and 5c and Figures S3.4.5-S3.4.8). The largest reductions in PMC were in Asia (~40–75 %), Australia (~20–30 %), South America (~20–50 %), and northern and southern European cities, with a few exceptions, such as Milan, western European cities, and Los Angeles. The reductions in PMC were larger and more uniform in Asia than in the rest of the world. As PMC is usually associated with local sources as well as LRT of dust, the observed reductions in PMC were due to the reduced non-exhaust traffic emissions and construction activities in the absence of LRT events. Chinese cities (e.g., Beijing, Jinan and Shenyang) and Spanish cities (Madrid and Valencia) —which recorded enhancement in PM$_{2.5}$ during full lockdown— reported reductions above 50% in PMC over the same period. For 2020 lockdown periods compared to 2015–2019, the meteorological conditions in these regions favoured secondary PM$_{2.5}$ formation leading to a rise in PM$_{2.5}$ (i.e., positive anomaly), whereas the restrictions on construction and traffic activities resulted in less resuspended dust, yielding negative PMC anomalies. In the case of cities impacted by LRT of dust, such as Spanish and Dutch cities, London, Augsburg and Munich, we observed enhancements in PMC during 2020. However, during the full lockdown in Spain, Querol et al. (2021) quantified PM variations after subtracting the contributions of Saharan dust and noted that the decrease in PM$_{10}$ was attributed to the reduced emissions of non-exhaust traffic and construction works.

We find a weaker positive correlation (excluding dust storm events) between PMC and mobility change (Figures S3.1.4-S3.1.6) when

considering all cities. However, when the data is examined just for Asian cities, a stronger correlation is observed (Figure S3.1.5) which indicates that traffic restrictions can reduce the PMC from dust resuspension and other non-exhaust emissions. Moreover, this finding also highlights the widespread problem of road dust in cities, that requires specific control measures.

Changes in the $PM_{2.5}/PM_{10}$ ratio were analysed to identify potential sources. A higher $PM_{2.5}/PM_{10}$ ratio means larger contribution from primary and secondary $PM_{2.5}$ whereas lower ratio indicates contribution from resuspended dust or LRT dust. The increase in the $PM_{2.5}/PM_{10}$ ratio (Figures S3.4.3-S3.4.4) was observed for Chinese, Indian, a few European cities (Helsinki, Milan, Moscow, Barcelona, and Madrid) and South American cities (Bogotá and Lima); however, a substantial decrease in PMC for these cities suggest that the increase in $PM_{2.5}/PM_{10}$ ratio was associated with the decrease in the coarse fraction of PM. The cities which recorded increases in $PM_{2.5}$ and $PM_{2.5}/PM_{10}$ ratio (e.g., Beijing, Shenyang, Xian, Madrid and Valencia) could have been impacted by secondary PM formation during the lockdown period due to meteorological conditions (e.g., increase in RH). The cities showing a decrease in $PM_{2.5}$ and an increase in $PM_{2.5}/PM_{10}$ ratio (e.g., Indian cities, Chinese cities other than Beijing, Shenyang, and Xian) had a substantial reduction in dust resuspension. In contrast, the cities impacted by LRT of dust (e.g., London, Augsburg, Munich, Milan, Amsterdam, Den Haag, and Rotterdam) showed a decrease in $PM_{2.5}/PM_{10}$ ratio. There were only a few cities (Seoul, Melbourne, Los Angeles, São Paulo, Santiago, and Quito) which showed a decrease in $PM_{2.5}/PM_{10}$ ratio where the decrease in fine PM was larger than the decrease in PMC.

(iv) Relative changes by type of environment

Most of the PM data used here were from monitoring stations at traffic or urban background locations, and only a few were located at industrial and rural sites. In general, we observed consistent changes in PM across all types of environments in the same city, particularly for $PM_{2.5}$, suggesting a strong regional influence on $PM_{2.5}$ as reported earlier (Singh et al., 2014). Our analysis demonstrates that while the lockdown restrictions can potentially reduce urban $PM_{2.5}$ concentrations, the benefits can be offset by LRT dust intrusion and biomass burning events, including increases in residential wood burning, or unfavourable meteorological settings (e.g., stagnant conditions) and/or secondary PM formation.

3.4.2. Nitrogen dioxide

(i) Nitrogen dioxide concentrations for 2015–2019

This section focuses on NO_2 as NO is included in the O_3 discussion in Section 3.4.3 and NOx is discussed as part of the OX analysis in Section 3.4.4. There was a strong variability in NO_2 concentrations between cities. Over 2015–2019 for the equivalent lockdown time periods, NO_2 concentrations were consistently higher in all Chinese cities as compared to the other cities and regions (Figure S3.4.9a). All sites showed inter-annual variabilities, though a general seasonal cycle can be seen in many of the cities (Figure S3.4.9b). Many NH cities showed decreasing NO_2 concentrations in 2015–2019 from their equivalent pre-lockdown time to the full relaxation period (i.e., decreasing NO_2 concentrations as the season transitioned from winter to summer). Indian cities (except Amritsar and Chennai) exhibited lower NO_2 concentrations in the partial relaxation period compared to the pre-lockdown period. In addition, no decrease across seasons was seen in Mexico City or in Bogotá. For Mexico City, the averaging periods used in this analysis are not aligned with the usual summer and winter seasonal cycle for NO_2 (García-Franco, 2020). As discussed in Section 3.3, for Bogotá, the biomass burning period extends across pre-lockdown and full lockdown periods (e.g., February–April) (Rincón-Riveros et al., 2020) and thus it would be expected that concentrations would be high across these two periods. Decreases were seen in NO_2 concentrations in Bogotá during the partial relaxation period of 2015–2019 compared to 2020.

The SH cities, other than Quito, showed increases from pre-lockdown

through partial relaxation in their multi-year means of 2015–2019 (i.e., increasing NO_2 concentrations from summer to winter). For Quito, a consistent seasonal cycle was not observed between pre-lockdown and full lockdown; however, annual mean NO_2 concentrations during the equivalent partial relaxation were 2–5 μg/m^3 lower than pre-lockdown period for 2015–2019.

(ii) Relative changes in 2020 NO_2 concentrations compared to 2015–2019

During the pre-lockdown period, for most cities, the mean NO_2 concentrations in 2020 showed a negative anomaly compared to the mean of 2015–2019 (Fig. 5d, S3.4.9c-d and S3.4.10). As discussed in Section 3.2, this could have been driven in part by favourable meteorological conditions in many cities. Six cities, however, showed positive anomalies in 2020 compared to the 2015–2019 means: Shenyang (14%) and Urumqi (7.6%) (China), Bengaluru (27%), Chennai (3%), and Kolkata (27%) (India), and Bogotá (6%). The differences are within the inter-annual variation for this period for 2015–2019 for all cities, except Bengaluru (Figure S3.4.9b-d).

All cities showed a decrease in NO_2 concentrations in the full lockdown period relative to the same period in 2015–2019 (Fig. 5d and S3.4.10), with twenty cities showing a 50% or greater reduction (Fig. 5d and S3.4.10); no cities experienced 50% or larger decreases during pre-lockdown. As discussed in Section 3.1, a clear positive correlation ($R^2 = 0.513$, Fig. 3) between changes in NOx and mobility for cities suggests that the reduction in NOx was largely driven by the reduction in vehicular emissions, as also shown by recent studies (Guevara et al., 2021; Biswal et al., 2021).

While the pre-lockdown relative anomalies (in %) were negative for most cities, they were larger for full lockdown than in pre-lockdown for all but eight cities (five cities in the Netherlands, Chandigarh, Augsburg, and Vancouver). The five cities in the Netherlands received on average more precipitation in the pre-lockdown (2.5–3.1 mm/day) as compared to BAU, while lower rainfall rates (0.06–1.3 mm/day) were recorded in the full lockdown compared to BAU, which can explain this difference. For Vancouver, this was driven by smaller decreases at the urban background site (-15% pre-lockdown and -9.3% full lockdown), while the traffic site did see larger decreases as expected during full lockdown (-14%) compared to pre-lockdown (-12%) (Figure S3.4.9e for full lockdown). For the other cities, the traffic sites did see a smaller decrease during full lockdown than that seen in pre-lockdown, though the larger changes were seen at non-traffic sites. Of these exceptions, only Vancouver and Chandigarh appeared as an outlier when the NO_2 anomaly is compared to change in mobility for full lockdown in Figure S3.1.3.

As the pandemic lockdown measures continued, only 50% of the cities provided data for a full relaxation period primarily because restrictions had not been removed in those cities and hence did not yet have a period considered to be 'full relaxation'. All cities, except for Tallinn and Shenyang, showed negative anomalies for the full relaxation (Fig. 5d and S3.4.10). For Melbourne, Sydney, Nicosia, Tallinn and Utrecht, these anomalies were within the inter-annual variability seen in 2015–2019 (not shown). The decrease for Beijing was larger during the full relaxation period in 2020 (-51%; -27 μg/m^3) than even in the full lockdown (-31%; -15 μg/m^3). For all other cities, larger decreases were seen in full lockdown compared to the full relaxation period.

(iii) relative changes by type of environment in full lockdown

Decreases were seen in full lockdown for all site types in all cities, except for rural sites in Tartu) (Figure S3.4.9e). As expected from the changes in mobility, the largest decreases in NO_2 were observed during full lockdown at the traffic sites, except for seven cities (Greater Gauteng, South Africa, the Chinese cities of Beijing, Chengdu, Shenyang, Urumqi, Wuhan and Zhengzhou), which saw larger decreases at other types of sites. The South African traffic site is located within a large industrial area (VTAPA area; DEAT, 2006) and is impacted by numerous sources. Beijing, Chengdu, and Shenyang saw the largest decreases compared to BAU at their rural sites. Urumqi and Wuhan saw the largest decreases at their urban background sites, and Zhengzhou at its

industrial sites.

3.4.3. Ozone

(i) Ozone concentrations for 2015–2019

We discuss here the changes in the maximum daily 8-hr mean O_3 concentrations (referred to herein as "O_3 concentrations" for simplicity). As daylight MDA8 and daily means of NO_2 and NOx are not equivalent in terms of time periods, we do not compare these directly. The use of daily mean values of NO_2 and NOx (discussed in Section 3.4.2) is to indicate the overall changes (e.g. decreasing in this case) during the lockdown periods and not to link directly to the MDA8 value. The MDA8 metric was chosen as it reflects the WHO guideline for O3 which was important to assess the implications of air quality under reduced emission scenarios (see Section 4.2). Considering all the cities in this study, the mean O_3 concentrations in 2015–2019 globally were recorded in the equivalent full and partial relaxation periods in Los Angeles and southern Europe (100–129 µg/m^3), coinciding with their peak O_3 season of June–July. For SH cities, such as Melbourne, means of 100–117 µg/m^3 were observed in the equivalent pre-lockdown period. For India, the means were 100–115 µg/m^3 before the monsoon period (equivalent pre-lockdown and lockdown periods) and for Mexico City high concentrations (90–105 µg/m^3) were observed for all the periods, with many other cities frequently exceeding the daily maximum 8-hr mean concentration of 100 µg/m^3 recommended by the WHO Air Quality Guidelines (Figure S3.4.11).

The Chinese cities reported very high O_3 concentrations during March and April in 2015–2016, despite this period not being the peak O_3 season, but mean concentrations decreased in 2017–2019. A probable explanation is the impact of national policies to curb industrial and traffic emissions, combined with the unfavourable meteorology in 2015–2016 for the increased production of O_3 (higher humidity and low insolation anomalies, see Section 3.2 and Figures S3.2.3-S3.2.4). Ozone concentrations in South Korea were markedly lower than in China. There was no evident inter-annual variation which indicated that the trends seen for Chinese cities might be attributed to the abatement of precursor emissions more than to regional meteorology trends. This would have similarly affected eastern China and South Korea. The Brazilian, South African, central and north European cities as well as New York reported 70–95 µg/m^3 for most of the periods, while Augsburg and Munich recorded markedly lower concentrations (38–76 µg/m^3) for the highest O_3 period in the full relaxation, as did the western South American cities (15–60 µg/m^3, excluding 75–86 µg/m^3 in the pre-lockdown in Santiago de Chile).

(ii) Relative changes in 2020 O_3 concentrations compared to 2015–2019

During the pre-lockdown period, O_3 increased generally in central and northern Europe (up to 44%, Fig. 5e, S3.4.11 and S3.4.12), most likely due to both the anomalously lower NO concentrations (up to -75%, Figures S3.4.13 and S3.4.14), reducing O_3 titration, and to the temperature anomaly (as a proxy for higher photochemistry that enhances O_3 formation) of up to more than 2.5 K in Berlin and Stockholm, and 3.6 K in Moscow (Monks et al., 2015) (see Figures 4 and S3.2.8). This was also observed in South Korea and South America, with only Rio showing a marked decrease, probably in part caused by intense titration, as it was the only South American city with increased NO concentrations (51%) from 2020 compared to the mean of 2015–2019. Conversely, modest O_3 decreases were observed in most southern European cities, except for Barcelona. In the Indian and North American cities, a mixed pattern was observed with substantial decreases in Montreal and Pune and increases in Chennai (Fig. 5e, S3.4.11 and S3.4.12). In other areas, such as Australia and South Africa, decreases were substantial, possibly due to the synergetic effects of lower temperatures and solar radiation (which inhibit O_3 production) and higher humidity and precipitation (see Belan and Savkin, 2019; Kavassalis and Murphy, 2017). Warm and humid anomalies prevailed over China in January (Figure S3.2.1) which explains why O_3 increased in most Chinese cities, except for Guangzhou,

Zhengzhou and Urumqi).

Similar variation patterns appeared in the full lockdown, with a general O_3 increase in central and northern Europe (between 10 and 29%), South Korea and South America (up to 67%) (Fig. 5e and S3.4.12). Again, Barcelona recorded an increase like those observed in central Europe. Marked decreases persisted in other cities, such as in most southern European and Canadian cities and South Africa. Minor changes were observed in Rome, Valencia, Calgary, Québec City, Vancouver and the Australian cities. As for the pre-lockdown, changes in O_3 were not observed in Mexico City, New York and Los Angeles. Mexico and Los Angeles (where heatwaves occurred in late spring/early summer in 2020), and specific sites of Barcelona, Pune and Delhi exceeded the WHO guidelines in the full lockdown (see also Section 4.2). A strong and general increase was observed in the Chinese cities, which reversed the pre-lockdown negative anomalies (all cities but Guangzhou and Beijing). Le et al. (2020) and Sicard et al. (2020) attributed this increase to the lower titration caused by the abatement of NO concentrations and to the non-linear relationship between NOx and VOC (in VOC-limited O_3 formation regimes, a decrease in NOx might prompt an increase in O_3, see Monks et al., 2015 and references therein).

Increases were also observed in rural areas where NO is expected to be very low. This increase in O_3 might have had an influence on the formation of secondary PM, which also was enhanced during the lockdown periods in several cities, which in some cases was attributed to higher humidity and stagnation, but in others to the enhancement of the oxidising patterns of the atmosphere associated with higher O_3 levels (Wang et al., 2020a). Most Indian cities included in this study, however, reported decreases in O_3 during the lockdown, except for Kolkata and Pune. Furthermore, it should be noted that while O_3 concentrations over the Indo Gangetic plain have generally decreased during daytime, enhanced night-time O_3 concentrations have been reported by Singh et al. (2020), illustrating the importance of diurnal variability.

The different O_3 variation patterns in central and southern Europe in the lockdown were also observed by Ordóñez et al., 2020 and Deroubaix et al. (2020), who attributed the higher O_3 concentrations in central Europe to anomalously high temperatures, low specific humidity and enhanced solar radiation (see Figures 4 and S3.2.8, Sections 3.2). In contrast, O_3 reductions in southern Europe were consistent with anomalously low solar radiation and high humidity, as well as to the weakened zonal wind (see Figures 4 and S3.2.8, Sections 3.2 and S3.2), which limited the advection of regional O_3. Similar patterns found in the pre-lockdown also support these meteorological effects.

Despite coinciding with the O_3 season in Europe and North America, the relaxation periods were marked by decreases in O_3 concentrations in most cities of these regions, except for Seville, Tartu and the Dutch cities, which showed either no substantial changes or modest increases. Most Chinese cities also exhibited a general decrease in the relaxation periods in 2020 compared to 2015–2019 (March–April), which is not the O_3 season but does coincide with the full lockdown in most countries. Only Urumqi showed higher O_3 concentrations. In India, a mixed pattern was observed, with marked decreases in Bengaluru and Delhi, and increases in Pune, Kolkata and Chennai. Differences in VOCs or NOx limitations for O_3 formation might account for these contrasting patterns but would need to be investigated through process-based modelling analysis.

The relaxation phases in the SH cities were out of the usual peak O_3 season (September– November) as shown for example by Cooper et al. (2014). In some SH cities (South American and South African for example), however, O_3 period can extend to or even peaks in the warmest months (December–January) (e.g., Govender and Sivakumar, 2019; Seguel et al., 2020). In non-urban sites, O_3 concentrations can also increase due to precursors being emitted during biomass burning events. In South America, three out of five cities reported increased O_3 concentrations, with only Rio de Janeiro behaving differently showing no major changes, as was the case for the Australian and South African cities. Over the 2020 analysis periods, Los Angeles and several South European cities exceeded the WHO air quality guidelines in the

relaxation periods (see also Section 4.2 and Figures 9 and S3.4.11).

The general O_3 decrease in most Chinese cities spanning a wide area, and under different meteorological anomalies, might be partly attributable to the decrease in emissions of precursors (NOx-limited O_3 formation). This is also probably the case of a large fraction of southern European and North American cities in the relaxation periods (June–July, and May for Canada, coinciding with the O_3 season in the NH). As shown in Fig. 3, the mobility changes in the partial relaxation of the Canadian cities, Naples and Rome (the only relaxation stage for these) ranged from -18 to -40%. In the full relaxation for the remaining southern European cities the anomaly ranged from -17 to -28%, except for Valencia which exhibited an anomaly of +11%. Moreover, the decrease in precursors was driven by the reduction in mobility, which reached 20% in most cities during full relaxation, indicating that such reductions during the O_3 season can have a clear impact on concentrations. The wetter and overcast conditions in June in southern Europe may have also contributed to the decrease in O_3 during the relaxation periods. Querol et al. (2021) applied machine learning meteorological normalisation to O_3 time series and found a generalised decrease (on average, -10%) in O_3 concentrations at receptor sites close to cities in eastern Spain. Thus, despite the role of meteorology in decreasing O_3, it seems that the reduction in emissions of precursors also contributed to abate O_3 pollution in the relaxation period.

For the Chinese cities, the general decrease found in the relaxation stages, shown in Figures 5, S3.4.11 and S3.4.12, (March–April) coincides with the occurrence of favourable meteorological conditions for O_3 production (positive insolation and negative RH anomalies over most of China, Figures S3.2.3–S3.2.4). Hence, we hypothesise that the decrease in O_3 was mostly due to a decrease in precursors. Mobility was reduced in all cities: between -20 and -86% in the partial relaxation and up to -58 % in six out of eight cities where mobility data were available. For these cities, it is also interesting to note that Chengdu recorded the largest decreases and the lowest increases for all periods, while Urumqi (a site in the Taklimakan desert, where high insolation anomalies were observed in both the lockdown and relaxation periods) and Zhengzhou (located in a humid and forested region of the Sichuan province) recorded the largest increases and lowest decreases, possibly indicating NOx- and VOC-limited O_3 environments, respectively.

In most periods, the South Korean cities and most South American cities recorded O_3 increases, pointing to a VOC-limited O_3 production regime. In Bogotá, the O_3 increase seems associated with the decrease in NOx (these two being anticorrelated with R = -0.42; *p*-value of 0.03), pointing to a VOC-limited O_3 regime, or an effect of less titration of O_3 due to a decrease in NO. Zambrano-Monserrate and Ruano (2020) reported an increase in O_3 in Ecuador during the lockdown and attributed it to the higher insolation caused by the $PM_{2.5}$ decrease. However, in Quito, an increase in O_3 was observed generally and for all the periods (pre-lockdown to relaxation), and not only in the full lockdown. Rio de Janeiro showed marked decreases in the pre-lockdown and lockdown, as did the South African urban area, pointing probably to a NOx-limited O_3 regime at these sites. Indian cities showed a mixed pattern, probably due to the different O_3 formation chemistry.

(iii) Relative changes by type of environment

Relative O_3 changes in 2020 (Figure S3.4.11e) did not show consistent patterns for the pre-lockdown and lockdown stages across the different site types, which is mainly due to different O_3 formation regimes. Although O_3 is expected to increase close to roadsides due to reduced titration when NO concentrations decrease, this behaviour did not prevail across all the cities studied. In southern Europe (especially Spain) and China, rural-receptor sites exhibited a marked relative O_3 decrease in the relaxation stages than other site types (between -20 and -36% in most Chinese rural sites, -13 and -18% at Spanish sites, and -7 and -10% at Tartu and Helsinki rural sites). Comparatively, the O_3 changes at other Spanish sites ranged from + 1 to -9%. A possible explanation is that the decrease in O_3 precursors in these cities caused a reduction in O_3 concentration in the conurbations, with pronounced

effects at the downwind rural sites.

3.4.4. OX analysis: Connecting changes in NO_2 and O_3

Because of the high NOx emissions in urban areas, it is expected that VOC-limited O_3 scenarios will prevail in metropolitan areas. Moreover, because NO emissions are reduced during the lockdown, the O_3 depletion by titration should decrease accordingly. Hence, providing a global overview of O_3 changes associated with the decrease in emissions during the COVID-19 lockdown is considerably more challenging than for most of the other pollutants. Fig. 6 summarises the daylight O_3, NO_2 and OX mixing ratios (in units of ppb) as boxplots for the 2015–2019 (blue boxes) and 2020 (red boxes) periods. The OX mixing ratios decreased in both urban and background environments, even in the same city, but with different intensities (for example, -12 and -24% at Rome Cipro and Guido, respectively). The only exception was Sydney Rozelle station with an increase of 2.4%. Grange et al. (2021) reported modest mean increases in OX when pooling all data from the European sites they investigated. However, they showed that the changes were city-dependent, with drops between -2 and -24% in Spain, Portugal, Italy and the United Kingdom. Shi et al. (2021) also found varying changes in OX at European sites during the lockdown (for example, -7.2% in Milan and +1.8% in Berlin), while reporting negative changes in Wuhan and Delhi. In our analysis, the OX also decreased in Wuhan (-5%) and much more in Delhi (between 20 and −42%). The intercomparison with other global sites was not possible due to the lack of similar studies, but we provide a summary of our data analysis in Table S3.4.1.

The slopes of linear regressions between the OX and NOx mixing ratios ($OX = NOx·\alpha + \beta$) changed considerably across the cities when comparing 2015–2019 and 2020, with background sites showing large increases (for example, from 0.44 to 11 at Madrid El Atazar, and from 0.59 to 2.80 at Chilbolton). However, the impact on the OX (via NOx. α) at these sites is small given the 21% and 37% drops in NOx concentrations at El Atazar and Chilbolton, respectively. Urban sites, such as Barcelona Eixample, showed modest changes in α (from 0.19 to 0.23), which, on the other hand, caused a substantial decrease in the local OX due to the 52% reduction in NOx. Regarding the regional contribution, the most outstanding changes from 2020 to 2015–2019 occurred at background sites (between 28 and 56%) in Madrid (El Atazar, from 48 to 21 ppb), and Rome (Guido, from 47 to 34 ppb). Urban sites in London and Wuhan presented small changes (between 2 and 7%) (from 50 to 49 ppb and 41 to 38 ppb, respectively) or null changes (São Paulo Pinheiros, no change to 32 ppb).

We observed that as NOx increased so did NO_2, which led to a larger fraction of OX in the form of NO_2 (NO_2/OX) irrespective of the site or whether considering 2015–2019 or periods with reduced mobility in 2020. At urban sites, this is due to the direct NO_2 emissions, while at background sites it is due to secondary formation. However, the partitioning seems to fall into two groups: i) urban sites exhibiting not only larger mean NO_2/OX ratios, but also a substantial decrease between the two periods (e.g., Eixample, from 0.53 to 0.33; Marylebone from 0.78 to 0.45, and Pinheiros from 0.56 to 0.38); and ii) background sites, with low NO_2/OX ratios and modest changes between the periods (Tona, from 0.06 to 0.11; El Atazar from 0.04 to 0.03, and Chilbolton from 0.12 to 0.07).

Despite the reductions in the concentrations of precursors observed during the lockdown stages, O_3 still made up a large fraction of the oxidant at background sites. Yan et al. (2018) observed increases in background O_3 in the period 1995–2014 at 71 out of 93 EMEP sites, which they associated with a 35% reduction in anthropogenic NOx emissions in Europe. Comparatively, the reductions in the daytime NOx concentrations observed at our European background sites in 2020 were between −21 (Madrid El Atazar) and −50% (Barcelona Tona), which led to a decrease in OX but kept the fraction of O_3 (O_3/OX) approximately constant. This suggests that the NOx reductions observed in such a short time span had a larger effect on the O_3 concentrations than those
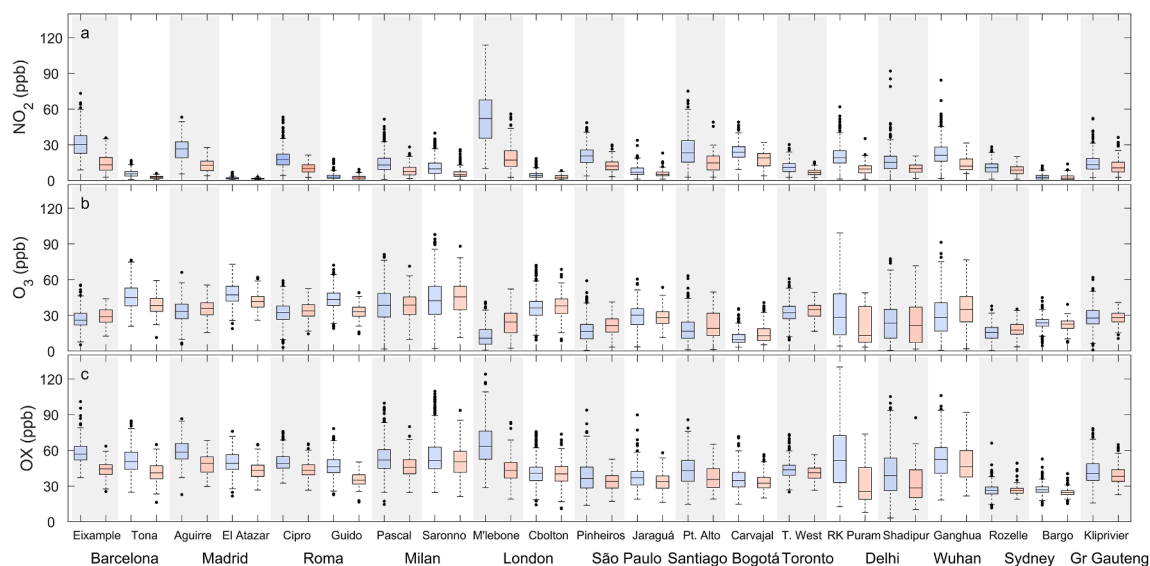
Fig. 6. Statistical summary of daylight O_3, NO_2 and OX mixing ratios for 2015–2019 (blue boxes) and 2020 lockdown periods (red boxes). The whiskers represent the 5th and 95th percentiles and the boxes are the interquartile range. Station types are given in Table S3.4.1. The grey shading is included to act as a visual aid. (For interpretation of the references to colour in this figure legend, the reader is referred to the web version of this article.)

reported by Yan et al. (2018) over 1995–2014.

3.4.5. Carbon monoxide

For the sake of brevity, we discuss here only the changes during the 2020 periods relative to 2015–2019. The analysis of changes during 2015–2019 and for different station types is given on section S3.4.

Relative changes in 2020 CO concentrations compared to 2015–2019 Most cities recorded lower CO concentrations in the 2020 pre-lockdown period with respect to 2015–2019, such as those in China, India, northern-central Europe, Canada, Australia and Mexico (see Fig. 5f, S3.4.17c–d and S3.4.18). In southern Europe, no spatial pattern was evident, with Barcelona, Naples, Milan and Nicosia showing decreases of up to -23% and Madrid, Seville and Rome showing increases of nearly +45%. In most South American cities, 2020 pre-lockdown concentrations remained similar to 2015–2019. The exceptions were for São Paulo and Santiago, where CO decreased and increased, respectively. The reasons for these regional contrasting variations for the two Latin American cities are unclear and warrant further investigation.

The general decrease in CO concentrations when comparing 2020 to 2015–2019 pre-lockdown, may be partly attributed to i) the effect of emission abatement policies reported previously for some countries, ii) the warm anomalies that occurred in some areas, such as Canada and Eurasia (probably leading to lower domestic heating emissions) and favourable dispersion conditions in continental Europe (see Section 3.2) in 2020. On the other hand, less favourable conditions for air pollution dispersion were observed in western and central Mediterranean countries (some Spanish and Italian cities) and would explain the higher CO concentrations compared to 2015–2019. Positive humidity and precipitation anomalies in southeastern Australia might partly explain the lower CO concentration in Melbourne with respect to 2015–2019.

A general decrease in CO concentrations was observed in the full lockdown compared to 2015–2019 in Chinese, Indian, South and North American, Australian and most of the European cities, except for the increases in two Spanish cities (Valencia and Seville) and Amsterdam. The CO decreases in Chinese cities (Fig. 5f and Figure S3.4.18) were not as large as in other areas, since the reductions in both mobility and industrial and energy emissions were small (see Fig. 3). Moreover, an increase in residential emissions was observed (Liu et al., 2020), despite the marked warm anomaly recorded over Eurasia (see Fig. 4 for April 2020 in the case of Europe and Figure S3.2.2 for February 2020 in the

case of China). Stagnant atmospheric conditions in the North China Plain (Li et al., 2020) inhibited dispersion and led to elevated CO concentrations (among other pollutants) during the first days of the full lockdown (Zhao et al., 2020), coinciding with the lowest CO decreases observed in NE China (-4 to -15%), which contrasts with other Chinese cities where the decreases ranged from -19 to -33%. Siciliano et al. (2020) and Dantas et al. (2020) attributed the CO decreases in the Brazilian cities mainly to the decrease in the light-duty vehicle traffic. The increases in CO concentrations in some Spanish cities can be attributed to domestic emissions (specifically biomass burning), associated with the cold anomaly that occurred over the Iberian Peninsula (see Fig. 4) and to agricultural biomass burning (Querol et al., 2021).

During the relaxation stages, CO concentrations remained lower compared to 2015–2019 in most areas, such as India, most of Europe and the Americas in partial relaxation and a few cities during full relaxation. China reported larger negative anomalies in the relaxation phase than in the lockdown periods. The largest decrease in CO during partial relaxation (middle February to end of March) in some cites (e.g., Beijing, Jinan, Shenyang and Zhengzhou) was associated to the decrease in SO_2, possibly related to reduced coal consumption in industries (Zheng et al., 2020; CREA, 2021), and favoured by mild weather (warm and dry anomaly, Figures 4 and S3.2.3) reducing residential heating. Conversely, CO concentrations were higher in Melbourne, Moscow, Amsterdam and Seville in the partial relaxation, and in the Estonian cities, Nicosia and Madrid in full relaxation.

3.4.6. Deciphering non-traffic contributions

To examine the influence of agricultural and biomass burning, we examined the changes in NO_2/CO ratio (Figures 7, S3.4.19 and S3.4.20). A large ratio indicates traffic dominated conditions in the cities and a small ratio indicates contributions from other sources, such as domestic/agricultural/wildfire burning. The use of NO_2 instead of NO_X was adopted because some cities did not provide NO data (including Chinese and Korean cities, Naples, Quito and Lima). However, the NOx/CO analysis is shown in Figures S3.4.21–S3.4.22 and S3.4.27 for cities with available data. In our study, we consider daily means for CO and NO_2 (and NOx) assuming that most of NO_2 is produced by fast titration in the presence of O_3. We therefore have not considered any differences between day and night-time. We discuss below the changes in the ratios from 2020 compared to the 2015–2019 mean and then the changes between cities for the 2020 lockdown periods.

(i) Relative changes in NO₂/CO ratios for 2020 compared to 2015–2019

The lowest NO_2/CO BAU 2015–2019 mean ratio reached 0.04 ± 0.01 and 0.05 ± 0.02 for Asia and South American cities, while much higher mean ratios were observed for the European cities (0.09 ± 0.03) and North and Central American cities (0.08 ± 0.02) (Figure S3.4.19). Mean values as high as 0.17 and 0.14 were observed for monitoring sites in European cities and in Melbourne, and as low as 0.01 in Bengaluru and Chennai. Our analysis shows that more than 50% of the low NO_2/CO ratios from Asia and South America are probably attributable to the CO contribution of domestic and agricultural biomass burning and forest fires. Other factors, such high CO from industry and power generation or old gasoline cars, and high dieselisation (higher NOx from passenger cars) of the European fleet may also have contributed.

When considering the changes of NO_2/CO in 2020 with respect to BAU, we would expect the ratio to decrease as a result of reductions in mobility (hence reductions in NO_2). The smallest reductions were observed in North and Central Americas ($-13 \pm 12\%$), South America ($-14 \pm 20\%$) and North and Central Europe ($-18 \pm 13\%$). Asia exhibited relatively intermediate changes ($-32 \pm 17\%$ in China, and $-25 \pm 30\%$ in India); while the highest reductions were reached in Southern Europe ($-49 \pm 20\%$), and especially in the Spanish cities ($-61 \pm 20\%$) (Figure S3.4.19). The highest reduction in Spain is attributed to the dense cities with a high proportion of diesel passenger cars and the worldwide strictest mobility reduction (Liu et al., 2020); while the lowest reductions were associated with lax mobility restrictions and lower diesel cars proportions in the fleet. The ratio increased for Vancouver, Mexico City, Urumqi and Kolkata in 2020 full lockdown period compared to BAU by $+2$, $+7$, $+7$ and $+25\%$. The cause for the increase in the ratio is that NO_2 reduced moderately in all cases, -11, -37, 25 and -26% for the above cities respectively, which indicates that NO_2 sources (traffic) reduced less compared with CO associated sources. Seville, Valencia and

Pune reduced the ratios in 2020 full lockdown period compared to the corresponding BAU period by between -68 and -80%, indicating the highest impact of road traffic on NO_2 levels.

The analysis of the NOx/CO shows very similar results, to the NO_2/CO, with only Santiago and Bogotá showing a larger reduction 2020 with respect to BAU by a factor of 5–7 when compared with NO_2/CO (Figure S3.4.19 and S3.4.21). This indicates a large decrease of NO during the full lockdown is attributed to a high traffic reduction in a low oxidizing atmosphere.

(ii) Relative changes in NO₂/CO ratios between cities for 2020

Fig. 7 shows the correlation between mean NO_2 and CO concentrations in the full lockdown for cities grouped by regions. The cities are grouped around different regression lines yielding different NO_2/CO. Mean ratios of 0.0273 and 0.035 for India (six of the eight cities) and China (four of ten cities), 0.050 for Europe (twelve of fifteen cities), and 0.068 for the US, Canada and Australia (twelve of fifteen cities) probably reflect the typical traffic-related urban pollution at these sites. Furthermore, one or several cities in each geographical region lie at lower NO_2/CO ratios (for example, Seville: 0.022, Guangzhou, Wuhan, Xi'an, Jinan, Chengdu, Zhengzhou: 0.021–0.027, Chennai and Bengaluru: 0.011–0.013, Quito, Bogotá and Santiago: from 0.019 to 0.049). This shift might be attributed to the impact of agricultural and/or domestic biomass burning and/or forest fires, and other CO pollution sources (such as petrochemical plants close to Seville). Conversely, Moscow, Munich and Augsburg have a much higher NO_2/CO ratio (0.085–0.121) than most European cities. The fleet composition might also have a certain influence, but in the case of the outliers, they do not seem to follow any geographical pattern as, for example, the ratio in Mexico City is markedly different from Quito, Bogotá and Santiago, but close to most US and Canada cities. This outstanding pattern in Mexico City is probably due to a long track-record of controlling emission sources, including traffic (Parrish et al., 2011). Further investigation is
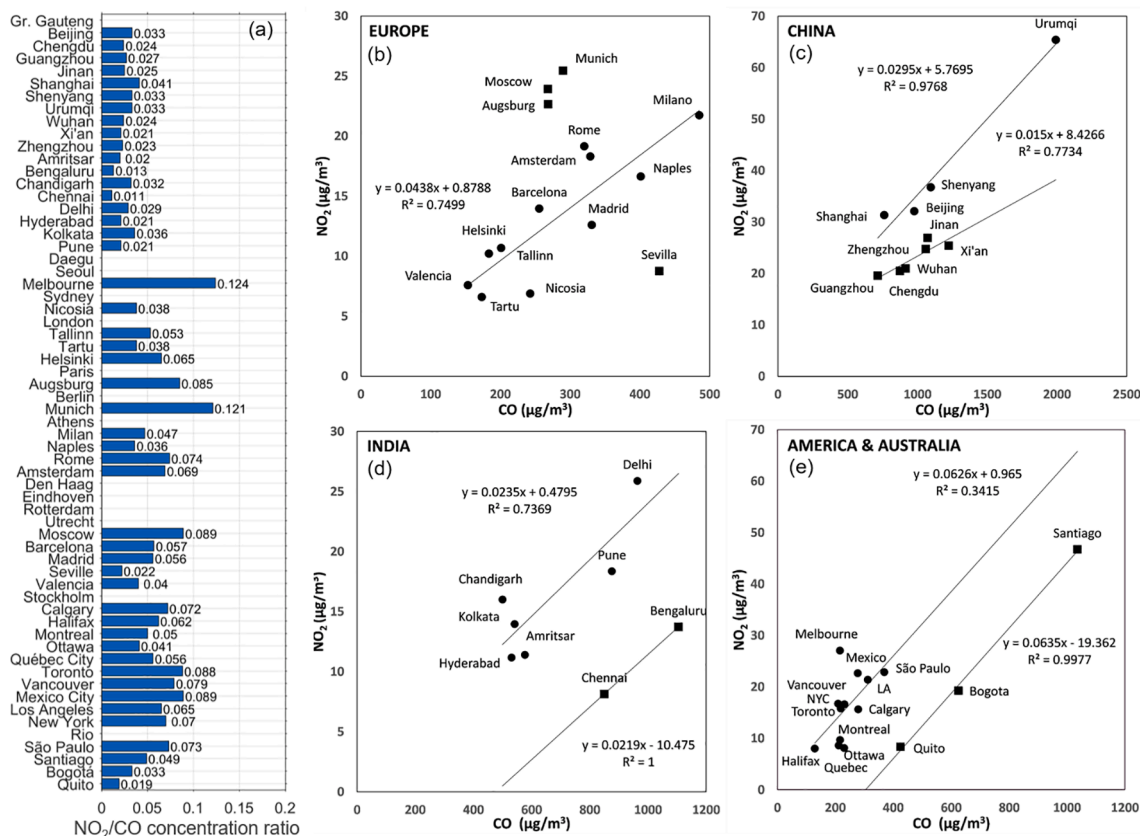
Fig. 7. Ratio of NO₂/CO as a mean over the 2020 full lockdown period shown as (a) bar plot for each city, and (b-e) cross correlation plots for the cities grouped by regions.

required to identify the causes of the higher ratios in German cities and Moscow compared to other European cities. For the cities where NOx data were available, we also observed similar NO_X/CO patterns as in the NO_2/CO analysis (Figure S3.4.27), except for Santiago, which fell into a case of traffic-dominated environment when using NO_X/CO, but into biomass burning-influenced when using NO_2/CO.

3.4.7. Sulphur dioxide

As in the case for CO, for the sake of brevity we discuss here only the changes during the 2020 periods relative to 2015–2019. The analysis of changes during 2015–2019 and for different station types is given on section S3.4.

Relative changes in 2020 SO_2 concentrations compared to 2015–2019

The SO_2 concentrations were generally lower in the 2020 pre-lockdown period compared with 2015–2019 (Figures S3.4.23 and S3.4.24). These falling trends were observed in all studied Chinese (−40 to −76%) and Australian (−36 to −40%) cities, most South and North American cities (−10 to −48%) and nine out of 13 European cities (−13 to −87%). In the case of Indian cities, the changes were mixed, with increases seen in Chennai and Hyderabad in 2020 during this period but no change was seen in Delhi. The changes of Indian cities are mixed, but during the full lockdown period, SO_2 anomalies were negative ranging from 13 to 27%.

In China, industrial coal boilers are major sources of SO_2 (Zheng et al., 2018a; 2018b). The large SO_2 reduction observed in China could be attributed to the strengthening of industrial emission standards, upgrading industrial boilers, and phasing out obsolete industrial capacities, which accounted for 43, 34, and 13% of the SO_2 reduction in 2013–2017, respectively (Zhang et al., 2019). Small changes in the SO_2 concentrations were observed in Valencia and Santiago (3.8 and 1.7%, respectively). For seven cities (Milan, Naples, Valencia, Ottawa, Rio de Janeiro, Quito and Chennai), SO_2 concentrations in the 2020 pre-lockdown were higher than the 2015–2019 averages (from 6.2 to 124%). Clearly, local meteorology also plays a role and it is possible that less favourable dispersion conditions could explain the increase in SO_2, for example for Milan, during the 2020 partial relaxation period compared to the corresponding period in BAU years. Moreover, the changes in OX were not negative worldwide meaning that oxidation was not the main reason for the changes in SO_2 during the pre-lockdown period. Besides, enhanced oxidizing capacity can promote the formation of sulphate by oxidising SO_2, and its increases can be understood as enhancements in the abundance of oxidants (e.g., OH) (Le et al., 2020; Shen et al., 2021). Hence, increased seasonal oxidation capacity in most NH cities while decreases in SH cities can be another cause for the opposite temporal variabilities in worldwide SO_2 levels.

All cities recorded negative SO_2 concentration anomalies during the full lockdown period with respect to 2015–2019 (i.e., lower concentrations in 2020), except for two Canadian cities (Calgary with 6% positive anomaly and Ottawa with 19%). The Chinese cities saw the largest negative percentage changes (−47 to −75%), followed by northern and western European cities (−28 to −55%), four out of the seven Indian cities (−0.1 to −27%), and all southern European cities (−3.6 to −39%). The South Korean (−20 and −36%), Australian (−18 and −22%), and most (12 out of 14) of the American cities (from −3.2 to −60%) also showed negative changes in the SO_2 concentrations. This indicated that the industrial sector in China was affected by the lockdown measures more than in other countries. In 2020, Santiago and Bogotá, which were among the SH cities considered in this analysis, registered reductions of 6 and 12% respectively while during the pre-lockdown period saw increases of 1.7 and 6.2%. This change indicates that lockdown regulations can reverse the emission trends.

Most countries registered negative changes in SO_2 concentrations during the partial and full relaxation stages in 2020 compared with the 2015–2019 averages, such as China (10/10, −17 to −78%), South Korea (2/2, −16 to −39%), Australia (2/2, −13 to −38%), most of the

European (9/13, −4.9 to −73%) and American cities (10/14, −4.8 to −46%). Conversely, the SO_2 concentrations were higher during the relaxation stages in 2020 in some Indian cities (4/7, 9.2 to 28%), Tallinn, Milan, Valencia, Halifax, Ottawa, Quebec City, New York, and Rio de Janeiro (5.5 to 74%). In addition to the unfavourable meteorological conditions, the SO_2 emissions in some cities have recovered to pre-lockdown level during the lifting period (Liu et al., 2020). However, interpreting individual cases is difficult in the case of SO_2 as a large fraction of the emissions are from point sources and the resulting plumes are subject to significant variabilities due to wind directions.

4. Implications for air quality policy

4.1. Regional changes in air quality during full lockdown

An overview of changes across countries and global regions is shown as box plots in Fig. 8 and Figure S4.1.1. On a regional basis South Asia (India) showed the largest decrease in mean PM_{10} concentrations (42%) during 2020 full lockdown period compared to the same period mean for 2015–2019. The decrease in PM_{10} for South Africa was 36%, and about 30% for East Asia (China) and South America. Australia and Europe exhibited decreases in mean PM_{10} during the same period of 2020 of 23% and 17% respectively. The two North American cities displayed the smallest decrease of just over 5%. However, as the number of cities analysed in Europe, East Asia and South America was larger, the spread of the values in these regions, expressed as the interquartile range (IQR), was also large (30, 24 and 23% respectively). This spread is mainly due to the different local emissions (e.g., via mobility and economic shut down) and responses to the pandemic lockdown as well as the varying influences of meteorology across the range of cities. For some countries the number of cities was small and hence it is difficult to generalise any conclusions. In the case of Spain (four cities) and Netherlands (five cities), anomalies of -25 and -5% were observed, respectively.

In terms of absolute values over the regions, $PM_{2.5}$ concentrations showed similar changes during the 2020 full lockdown period, except that the IQR values were smaller, with cities in South America exhibiting the largest value of 26%, East Asia showing 24% and Europe 20%. There was a universal reduction in the countries' $PM_{2.5}$ means, with the largest decreases for India (41%), 8.9% for China, 19% for the Netherlands, 11% for Spain, 9% for China and 5.3% for Canada. As discussed in Section 3.4.1, secondary aerosol formation may have influenced $PM_{2.5}$ changes in East Asia (China) (Wang et al., 2020b; Le et al., 2020), while European cities (mainly in Spain) showed some evidence that there may have been contributions from biomass burning, elevating the mean $PM_{2.5}$ concentrations during the 2020 lockdown. To arrive at a more robust conclusion, process-based modelling analysis will be able to elucidate the differences in the role of resuspension, LRT contribution and potential formation of secondary aerosols with drastic mobility reduction.

The coarse particulate matter fraction, which is particularly sensitive to reductions in local mobility, showed a complex response, with a general decrease in the 2020 means across the regions. East Asian cities displayed the largest reduction in PMC during the full lockdown period of 2020 (64%) with South Asian and South African cities showing a reduction of approximately 50% (Fig. 8c). However, dust transport can also significantly affect PMC concentrations. During 19–22 March 2020, a Sahara dust outbreak affected Spain and France, and another outbreak occurred over large parts of central and southeastern Europe during 26–28 March 2020, which may explain the increase in PMC in Germany and even the Netherlands (see Table S3.3.1 and S3.3.6). The large spread in PMC concentrations (Fig. 8c) for the countries is not unexpected as there are mixed contributions from local sources of dust as well as contributions from LRT.

As NO_2 strongly reflects changes in vehicle emissions, there was a universal reduction in the mean values in 2020 full lockdown period compared to the 2015–2019 means for all regions and countries in the
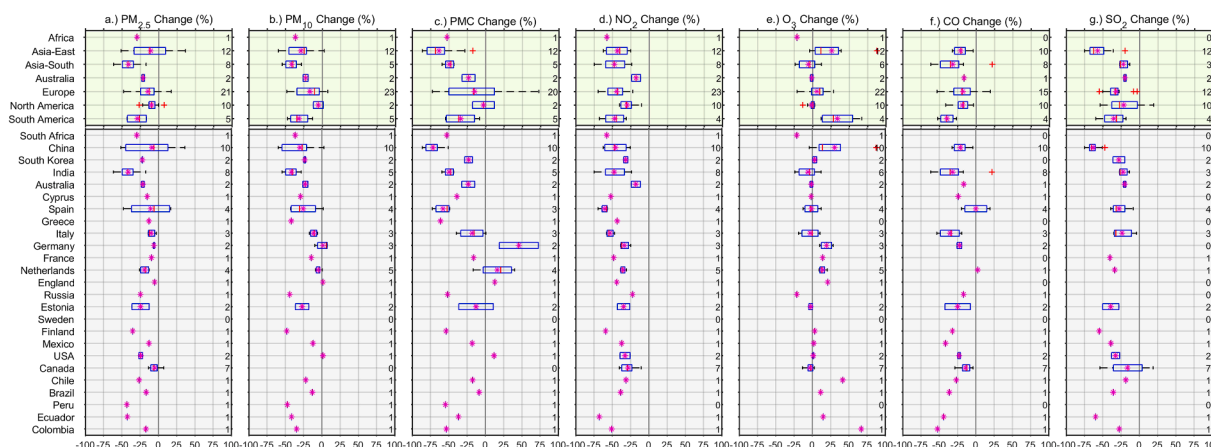
Fig. 8. Continental/country-wide changes in air pollution shown as boxplots for the full lockdown period for (a) PM$_{2.5}$, (b) PM$_{10}$, (c) PMC, (d) NO$_2$, (e) O$_3$, (f) CO, (g) SO$_2$. Numbers on the right-hand side of the panels indicate number of cities. The red line in the box shows the median value, magenta star indicates the mean value, and the box shows the interquartile range. The red + symbol is the outlier (values more than 1.5 times the interquartile range). (For interpretation of the references to colour in this figure legend, the reader is referred to the web version of this article.)

range from 18 to 68% (Fig. 8d).

As mentioned in Section 3.4.3, changes in O$_3$ showed a complex response. The mean reductions in concentrations were small in 2020 compared to the 2015–2019 mean for South Asia (India) (nearly 6%). Reductions were marginal for North America (1.6%) and Australia (1.3%) but with an indication of a larger negative anomaly for South Africa and large positive anomalies for East Asia (China) (26%) and South America (34%). For Europe, a small mean positive anomaly of 5.6% was observed.

In the case of SO$_2$, East Asia (China) showed a decrease of nearly 60% in the mean concentrations for 2020 compared to that of 2015–2019. A decrease of 35% for South America, 29% for Europe, 22% for North America and 20% for Australia were observed. Reductions in 2020 SO$_2$ concentrations compared to BAU were observed for all the countries reflecting the considerable reduction globally in industrial activities during lockdown periods.

CO showed universally negative anomalies during 2020 full lockdown period compared to the mean of 2015–2019 for all regions, with the largest decrease for South America of nearly 40% and the lowest negative anomaly for Australia of nearly 17%. These trends are reflected for all other countries, with only a marginal increase for the Netherlands which is most likely negligible considering the inherent uncertainties in observational data.

The NO$_2$/CO ratio, which was used to understand air quality contributions from combustion sources (e.g., biomass burning) other than road traffic emissions (see Section 3.4.6), also showed a decrease in the mean values for 2020 full lockdown period compared to the equivalent 2015–2019 period, from 16% in North America (excluding Halifax) to 32% in Europe. This decrease reflects the general reduction in mobility (hence reduced mean NO$_2$ concentrations). In specific cases discussed in Section 3.4.6 (for example, Seville and Valencia in Spain and Bangaluru in India), contributions from biomass burning plumes were identified by the higher mean CO concentrations which led to a lower ratio of % 11–22% during 2020 compared to 2015–2019.

4.2. Air quality changes compared to WHO guidelines

In order to understand the implications of the changes in air pollutant concentrations for human health, it is helpful to compare these changes during 2020 lockdown periods to health-based thresholds WHO guideline values (WHO, 2006). These guidelines are set to protect health, and thus an exceedance of the threshold could indicate that health is at risk.

The time periods of the different lockdown stages varied, presenting

a range of duration across cities. For pre-lockdown in this assessment, most cities considered 30 days, and for full lockdown the length ranged from 14 to 91 days. There is no direct equivalent WHO guideline (WHO, 2006) for such averaging periods. In the case of O$_3$, the analysis is based on the mean 8-hr daily maximum concentration across the lockdown periods. For the purposes of discussion below, the analysis does not represent actual exceedances of these guidelines but provides more an indication of the potential to assess the exceedances. Would the WHO guidelines have been met if the reductions or changes had occurred over a year (or appropriate averaging period)? To examine whether the reductions in anthropogenic activities imposed by the COVID-19 lockdown could potentially improve the air quality and meet the WHO guideline values, the mean lockdown values have been compared to the WHO guidelines in Fig. 9 and shown as a graphical global representation in Fig. 10. We do not consider CO in the discussion below as there is no WHO guideline value for this air pollutant.

For NO$_2$, over the BAU period, 27 cities had mean concentrations higher than the WHO annual mean of 40 μg/m^3 during at least one of the equivalent lockdown periods, with 17 cities exceeding 40 μg/m^3 during the equivalent full lockdown period (Fig. 9c). Our analysis shows that if the equivalent reductions observed during the lockdown periods of 2020 had occurred over the whole year, only two cities (Shengyang and Bogotá) would have still exceeded the guideline. Nevertheless, the concentrations were significantly improved compared to BAU (Fig. 9c). While all but one of the Chinese cities had mean NO$_2$ concentrations larger than 40 μg/m^3 during the full relaxation equivalent period in 2015–2019, only four cities did so in 2020. This illustrates that for NO$_2$, drastic reductions in urban road traffic would dramatically cut the exceedances of the annual NO$_2$ guideline value in cities. There are indications, however, that by the time of the full relaxation period, four of the Chinese cities had exceeded the WHO guidelines and several more were again approaching the limit values. This strongly suggests that measures need to be ambitious and must be implemented on the longer term for them to be effective.

While decreases in PM$_{2.5}$ and PM$_{10}$ were seen in many cities during full lockdown (Fig. 5, S3.4.1-S3.4.2 and S3.4.5-S3.4.6), most cities still had mean concentrations above the annual WHO guidelines during full lockdown (Fig. 9a and b). The decreases in mean PM concentrations for 2020 were smaller, with values well above guidelines for many regions, especially China, India, South Korea, South America and some European hotspots. As noted earlier, this indicates that if the lockdown measures had been implemented routinely, they still might not have been effective on their own to decrease PM concentrations below the WHO guidelines.

Marais et al (2017) and Wang et al. (2020c) have shown that

Fig. 9. Comparison of potential exceedance of WHO guideline values for BAU (2015–2019 means) and 2020 full lockdown periods for (a) PM$_{2.5}$, (b) PM$_{10}$, (c) NO$_2$, (d) O$_3$ (urban sites), (e) O$_3$ (rural sites), and (f) SO$_2$. The numbers represent the ratio between the lockdown period means and the WHO guideline values: annual PM$_{2.5}$ (10 μg/m^3), annual PM$_{10}$ (20 μg/m^3), annual NO$_2$ (40 μg/m^3), 8-hr daily maximum O$_3$ (100 μg/m^3) and 24-hour mean SO$_2$ (20 μg/m^3).
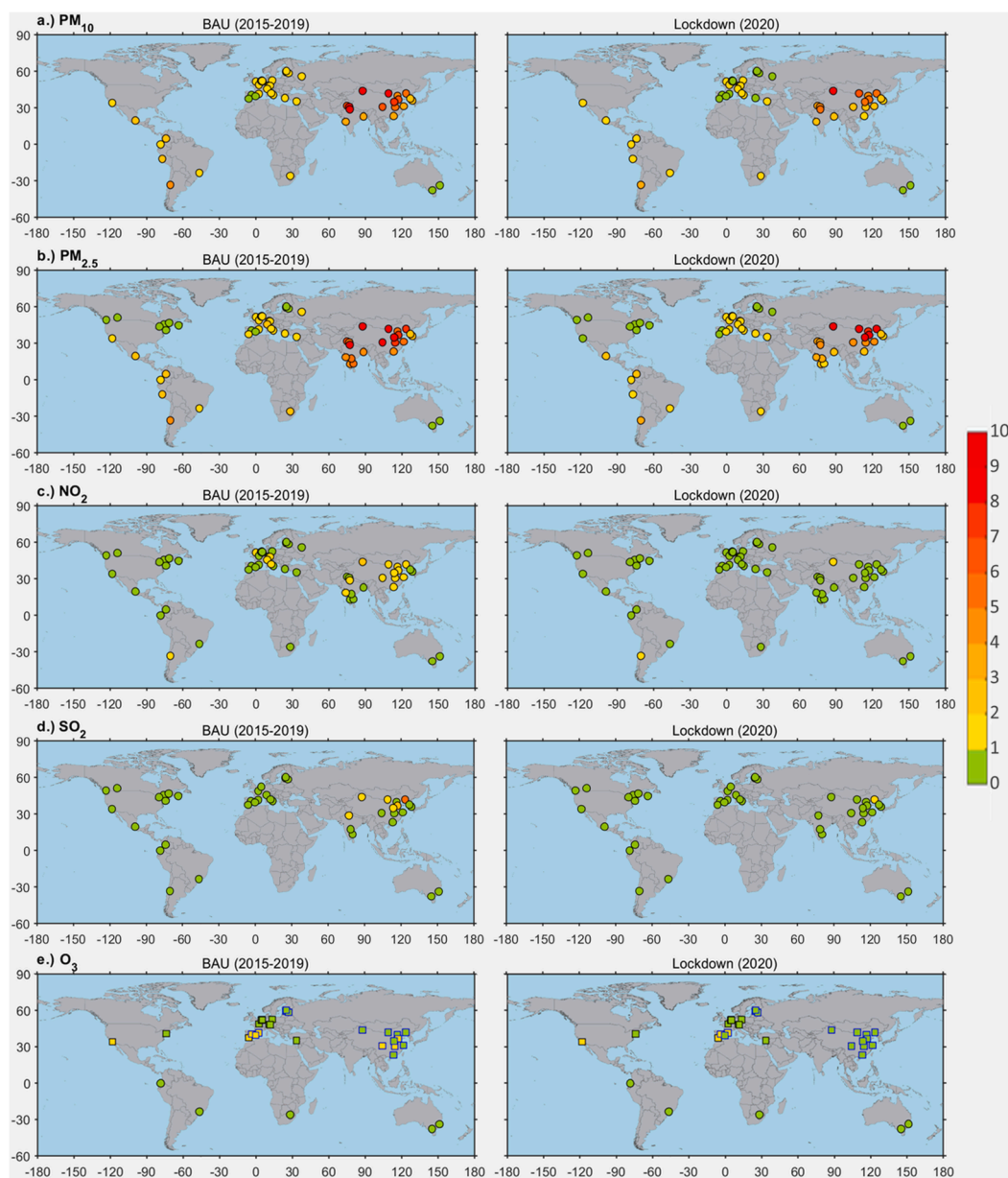
Fig. 10. Indicative exceedances shown as a ratio of mean observed concentration to the WHO guideline values for full lockdown period for (a) PM$_{10}$, (b) PM$_{2.5}$, (c) NO$_2$ and (d) SO$_2$ for cities worldwide. For (e) O$_3$, the indicative exceedances are shown for full relaxation period for Northern Hemisphere cities (squares) and for full lockdown period for Southern Hemisphere cities (circles) at background sites with black edges to represent urban stations and blue edges to represent rural stations. (For interpretation of the references to colour in this figure legend, the reader is referred to the web version of this article.)

decrease in SO$_2$ emissions can lead to a decrease in sulphate aerosols and also a decrease in secondary organic aerosol formation. Consequently, reductions in SO$_2$ could have been partly responsible for the reduction in PM$_{2.5}$ along with the changes in other precursors (e.g. VOCs) and influence of meteorological factors. As there is a lack of observational datasets for PM$_{2.5}$ chemical components, further investigations will be required to verify these possible linkages (Gkatzelis et al., (2021).

Lockdowns for most cities did not occur during peak O$_3$ period and for all but seven cities examined, the previous five-year mean O$_3$ concentrations were below 100 μg/m^3 during all the equivalent lockdown periods (Fig. 9d). Only Los Angeles and Mexico City had mean concentrations above 100 μg/m^3 in full lockdown in both the 2015–1019 and 2020 analyses. At urban background stations (Fig. 9d), four cities would likely exceed the WHO guidelines with additionally four more within 10% of the guidelines. In the case of rural locations (Fig. 9e), four rural stations would potentially exceed the 100 μg/m^3 WHO guideline

value during 2020 for these periods, and two more (Milan and Valencia) would be within 5% of the guideline.

In the case of SO$_2$, apart from some Chinese cities, concentrations at most locations were already below 20 μg/m^3 during BAU period (Fig. 9f). During both the pre-lockdown and the full lockdown periods of 2020, SO$_2$ mean concentration for only Shengyang was above 20 μg/m^3, though it was still lower than the equivalent BAU period. Over the relaxation periods in 2020, SO$_2$ mean concentrations were below the WHO guideline values in contrast to the 2015–2019 period.

4.3. Implications for local air quality management

Local air quality management relies on effective measures that can be applied within the boundaries of a city or even within areas of air quality abatement zones. When interpreting changes in air pollutant concentrations to design regulation strategies, many factors have to be

considered including NOx levels, reactivity of the VOCs, oxidant levels, along with the role of meteorology (Kroll et al., 2020).

There is clear evidence that local measures that significantly reduce traffic emissions, such as restrictions on traffic mobility, will be effective for decreasing NO_2 concentrations. As some cities required large reductions in mobility to attain a large decrease in NO_2 concentrations (i. e., up to -85%, Figure S3.1.3), the implication is that very ambitious polices would be needed to achieve and sustain these improvements on a long-term. Analysis of different station types revealed that the changes in mobility led to the largest decrease in NO_2 at traffic sites, as expected. On the other hand, results from this study suggest that such measures impacted the different PM fractions with varying degrees of outcomes. While we observed some decrease in the PMC fraction, generally associated with emissions from non-exhaust and other resuspension sources, there was considerable variability between cities. These measures, however, were not as effective for decreasing $PM_{2.5}$ and PM_{10} to meet the WHO guidelines. In the case of regional secondary species, however, the urban background plays a crucial role, and these species might increase in concentration independently of the drastic mobility reductions due to: i) meteorological conditions that favour secondary $PM_{2.5}$ (such as high humidity and atmospheric stagnation (Le et al., 2020) and O_3 (stagnation and high insolation) formation; ii) high regional NH_3 emissions (mostly from farming and agriculture) yielding high secondary inorganic PM (Backes et al., 2016); iii) higher O_3 concentrations, leading to higher secondary PM (Wang et al., 2020a); and VOC-limited O_3 formation regimes, potentially increasing O_3 when NOx concentrations are reduced (Monks et al., 2015). This has important implications for formulating and implementing future air quality policies. While local measures, for example, the reduction of road traffic, will lead to positive benefits in terms of ambient NO_2 concentrations, they must go hand in hand with regional measures to be effective in decreasing $PM_{2.5}$ and O_3 concentrations. In fact, the co-benefits will be maximised if these actions are coordinated with climate actions to reduce the emissions of short-lived climate pollutants and greenhouse gases, especially if these policies are oriented towards multiple sectors, including cleaner energy transition, low or zero emission traffic, and other control measures targeted at source.

4.4. Implications for regional and global air quality policies

Although progress has been made since the introduction of regional agreements, such as the United Nations Economic Commission for Europe (UNECE) Convention of Long-range Transboundary Air Pollution (CLRTAP) (e.g., vision and strategic priorities set out in the long-term strategy for the Convention for 2020–2030 and beyond, ECE/EB. AIR/142/Add.2, decision 2018/5), a considerable proportion of the world's population is experiencing high levels of air pollution. This is further supported by the recent second clean air outlook (EC 2021), which considers the impact and progress of meeting the National Emission reduction Commitments Directive (NEC Directive) by the European Union member states. It concludes that a significant proportion of the European population is exposed to air quality above the EU Air Quality Limit values and breathing air that does not meet the WHO guidelines. Our analysis of $PM_{2.5}$ and PM_{10} has shown that, despite drastic reductions in activity and mobility, large proportion of the global population will continue to experience air quality that exceeds the WHO guideline values even during conditions that mimic the full lockdown period. While our study corroborates the previous assessment conducted by Maas et al. (2016) on the impacts of the CLRTAP Convention, it does highlight the need to reassess if expected reductions from future (foreseen) policies adopting, for example, clean energy technologies and infrastructure, will provide similar levels of emissions reductions to those achieved during the lockdown periods and if they will be sufficient to improve the air quality to meet the WHO guideline values.

It also supports that coordinated regional and global responses will be required, for example, through the implementation of the Gothenburg Protocol (e.g., for PM and O_3 and their precursors, NOx, VOCs, methane, ammonia and SO_2), to reduce $PM_{2.5}$ levels while not exacerbating other air pollutants, such as O_3. This study demonstrates that meteorologically driven variations in $PM_{2.5}$ (e.g., via LRT of smoke and dust) may be larger than even the drastic emission reductions experienced during the full lockdown periods in 2020 and can lead to an increase in the regional background $PM_{2.5}$ concentrations affecting all site types. For secondary air pollutants, the combined role of non-linear chemistry and meteorology must also be considered in designing emission control strategies (e.g. Kroll et al., 2020). The evidence is starkly clear that science-based policy responses must take account of local, regional and even global scales when designing and implementing measures to cut emissions across different source sectors.

The drastic reductions in emissions across regions due to the responses to the pandemic (e.g., as shown by Guevara et al., 2021 for Europe) provided a unique opportunity to test the impacts of emission reduction targets stipulated in the Gothenburg Protocol. Critically, our analysis demonstrates that emissions targets might have to be even more ambitious beyond 2030 and be specific to different regions of the world. Consistent analysis of real-world air quality responses during the lockdown phase, such as this current study, will provide an invaluable resource to design and test the effectiveness of scenarios to implement regionally relevant emission reduction protocols through process-based studies. Given that this study clearly indicates that even drastic reductions in mobility would not be enough to significantly reduce $PM_{2.5}$ concentrations and meet WHO guidelines in many parts of the globe, reductions included in regional and global treaties may well have to be reassessed to include more ambitious air quality strategies streamlined for different regions and countries. Even in the case of NO_2, this study indicates that emission reductions equivalent to those during the full lockdown period might be required to meet the WHO guideline values (Fig. 9c).

Another aspect that is clearly demonstrated is that regionally dependent meteorological and episodic emissions from natural or anthropogenic sources (e.g., dust and biomass burning events) can add further complexity to assessing the impact of air quality policies and protocols. While there are efforts in place in regions such as Europe (extending to the Middle East and North African countries) and North America (e.g., San-Miguel-Ayanz et al., 2020) to combat and control forest and wildfires, it is necessary to tackle this problem from a global and cohesive perspective, since the occurrence of transboundary smoke may undermine local and region efforts to curb air pollution. Such an approach should, however, consider the differing role of fires where they can also be a factor in sustainability of ecosystems (e.g., grasslands).

4.5. Limitations of the study

The conclusions of this study should be considered in relation to the limitations of the analysis. Despite having data from 63 cities across the globe, locally verified measurements were not easily accessible or available for many countries, especially for much of Africa, Russia and the Middle East. For Europe, the number of cities was larger because official local ground-based measurements are publicly available. For the other countries, data were analysed for major cities in that region and treated as reflecting the general responses.

In order to avoid issues caused by the lack of consistent *in situ* meteorological measurements for the cities, this study relied on global reanalysis data which inevitably has a relatively coarse resolution. Depending on the local and national responses, the length of lockdown phases was different for different regions as well as the number of stations from which data was available, and these factors may also influence the uncertainty in estimating the air quality changes. Our analysis was limited to the effects on air quality until September of 2020 and did not consider lockdown measures implemented subsequently to address challenges posed by the second and even third wave of the COVID-19

pandemic. Finally, we did not examine the relationships between nationally imposed lockdown measures and the extent of public adherence or perception to these measures, and how these may have affected air pollution emissions in the different phases. Similarly, there may have been some redistribution in the mode of travel from public transport to private cars and cycling during the lockdown periods. Although this would be included implicitly in the mobility data, specific analysis of the impact of changes in the mode of travel, such as the ban on travel and the dramatic decrease in demand in the aviation sector, have not been addressed here.

5. Conclusions and recommendations

A globally consistent study using ground-based observations has been conducted to examine the changes in air pollution during COVID-19 lockdown periods. Analysis of the mobility data clearly showed the correlation with traffic-related pollutants, such as NO_2 and NOx and even for PMC for some cities. While almost universally significant improvements were observed in NO_2 during lockdown periods, any measures to be effective will have to be ambitious and implemented on a long-term basis. In addition, measures during partial lockdown would not be sufficient, and stricter measures as in the full lockdown period would be required to meet the WHO guidelines. Our analysis assumes that most of NO_2 in urban areas is produced by fast titration as soon as NO is emitted in the presence of O_3. There may, however, be effects that differ between daytime and night-time and these should be investigated with more detailed measurements for cities across the world. This study also indicates that measures as implemented during the lockdown phases would not be effective on the short term or on their own to decrease PM concentrations below the WHO guidelines, especially for China, India, South Korea, South America and for some European hotspots.

The O_3 changes observed in some areas were due to a combination of meteorological anomalies (leading to depletion of O_3) and emissions changes during the COVID-19 relaxation period (leading to a general decrease in O_3 in urban areas). This was particularly so for China and southern Europe, and in several cities in North America and India even when mobility (and hence NOx) was reduced. These effects were also evident in Rio de Janeiro, South Africa and other regions during the lockdown. However, in most South American and South Korean cities, a general O_3 increase was recorded in all the study periods, possibly indicating a VOC-limited O_3 formation environment. Also, in several cities, the lockdown caused an increase in O_3 due to weaker titration caused by the drastic reduction in NO concentrations. The effects of seasonality on O_3 become more evident when comparing cities in the Southern and Northern Hemispheres (e.g., Cooper et al., 2014) and when selecting the most relevant periods. In both hemispheres, there are many cities where reducing O_3 concentrations remains a challenge despite the emissions reductions in mobility and emissions during lockdown periods.

Analysis of different station types revealed that while the changes in NO_2 were driven mainly by reductions in on-road traffic, the urban background played a crucial role in the case of secondary species ($PM_{2.5}$ and O_3). Secondary air pollutants have a major regional origin and might increase due to specific meteorological conditions, high regional emissions of precursors, such as NH_3 and VOCs, or changes in the VOCs/NOx regimes and the oxidising atmospheric capacity. For this study, emission and concentration data for VOC was not included in the analysis as there are uncertainties in the available data and generally there is the lack of these specific datasets in many parts of the world (e.g. Gkatzelis et al., 2021). We recommend that further investigation be conducted to disaggregate NOx/VOC regimes as data becomes available. Similar to $PM_{2.5}$, O_3 anomalies exhibited large regional variations, with no overall changes in South Asia, Australia, and North America and small increases in Europe and positive anomalies in east Asia and South America (the largest positive anomaly was ~70% in Colombia). In order

to elucidate these regionally dependent heterogeneities, process-based modelling analysis will be required.

The larger daylight oxidant OX reductions were usually observed at urban rather than at rural background sites. This suggests that at the former sites, the decreases in primary NO_2 emissions outpaced the O_3 production, while at the latter sites the OX was mostly driven by the regional contribution and, to a lesser extent, by the reductions in local NO_2 and O_3 concentrations. These findings raise challenges for air quality management strategies, as they indicate that O_3 at background sites can only be combated if control measures go beyond local scales and by addressing, for example, regional transport.

Carbon monoxide does not generally feature in air quality management strategies, as concentrations have decreased substantially over the years. However, when examining biomass burning events (e.g., forests, solid fuel and waste), our analysis shows that CO concentration —even during lockdown periods— can exhibit an increase, highlighting the importance of sources that are often neglected when considering air quality in urban areas. The restrictions on mobility experienced during 2020 presented an opportunity to accelerate and adapt to different modes of work (e.g., e-working) and commute (e.g., increased use of bicycles) and to supplement the move towards lower emission transports. The realisation that society can operate in a new configuration could be considered as part of broader socio-economic strategies to further control air pollutant emissions in cities and meet the UN "Sustainability Cities and Communities" goal (SDG 11).

To understand how the interplay of local, regional and global measures will be most effective to improve air quality globally, process-based analysis will be required including, for example, the use of chemistry transport models. It seems particularly important to examine which combination of abatement measures (e.g., reductions in precursor emissions) would be effective and how these might be affected by complex meteorological and episodic conditions. Moreover, policies to reduce agriculture related biomass burning practices, use of solid fuels for cooking, and control wood-burning for domestic heating should be considered, including their social development implications. Our study highlights the importance of understanding how meteorologically driven influences and episodic emissions from natural or anthropogenic sources (e.g., dust, domestic and agricultural biomass burning events) can add further complexity to meeting air quality policies. These complexities add to the uncertainties in understanding how climate change might compromise future air quality on urban and regional scales, particularly for $PM_{2.5}$, O_3 and their precursors.

While local measures, such as the restriction of road traffic, will lead to positive benefits for NO_2, they must go hand in hand with regional measures to be effective for $PM_{2.5}$ and O_3, which have important implications for formulating future air quality policies. In relation to global responses (e.g., through the Gothenburg Protocol or future updates), the pandemic period represented a test case to assess, through process-based studies, if such responses will be sufficient to meet WHO guideline values or if more ambitious measures will be required to reduce $PM_{2.5}$ levels while not exacerbating other air pollutants, such as O_3. Critically, the evidence is starkly clear that even unprecedented reductions in mobility and economic activity was not sufficient as a transition to better air quality in many parts of the world. This suggests that a radical shift is required to develop more effective science-based policies which take account of local, regional and global scale influences and that cut across different source sectors.

CRediT authorship contribution statement

Ranjeet S. Sokhi: Conceptualization, Methodology, Validation, Formal analysis, Investigation, Writing – original draft, Writing – review & editing. **Vikas Singh:** Conceptualization, Methodology, Validation, Formal analysis, Investigation, Writing – original draft, Writing – review & editing. **Xavier Querol:** Conceptualization, Methodology, Validation, Formal analysis, Investigation, Writing – original draft, Writing – review

Declaration of Competing Interest

The authors declare that they have no known competing financial interests or personal relationships that could have appeared to influence the work reported in this paper.

Appendix A. Supplementary material

Supplementary data to this article can be found online at https://doi.org/10.1016/j.envint.2021.106818.

References

Backes, A.M., Aulinger, A., Bieser, J., Matthias, V., Quante, M., 2016. Ammonia emissions in Europe, part II: How ammonia emission abatement strategies affect secondary aerosols. Atmospheric Environment 126, 153–161.

Bauwens, M., Compernolle, S., Stavrakou, T., Müller, J.-F., Gent, J., Eskes, H., Levelt, P. F., A, R., Veefkind, J.P., Vlietinck, J., Yu, H., Zehner, C., 2020. Impact of coronavirus outbreak on NO$_2$ pollution assessed using TROPOMI and OMI observations. Geophys. Res. Lett. 47 (11) https://doi.org/10.1029/2020GL087978.

Belan, B.D., Savkin, D.E., 2019. The role of air humidity in variations in near-surface ozone concentration. Atmos. Oceanic Opt. 32 (5), 586–589.

Biswal, A., Singh, V., Singh, S., Kesarkar, A., Ravindra, K., Sokhi, R., Chipperfield, M., Dhomse, S., Pope, R., Singh, T., Mor, S., 2021. COVID-19 lockdown-induced changes in NO2 levels across India observed by multi-satellite and surface observations. Atmos. Chem. Phys. 21 (6), 5235–5251.

Brimblecombe, P., Lai, Y., 2021. Subtle changes or dramatic perceptions of air pollution in Sydney during COVID-19. Environments 8 (1), 2.

Buchholz, R., Hammerling, D., Worden, H., Deeter, M., Emmons, L., Edwards, D., Monks, S., 2018. Links between carbon monoxide and climate indices for the southern hemisphere and tropical fire regions. Journal of Geophysical Research: Atmospheres 123 (17), 9786–9800.

Caseiro, A., Bauer, H., Schmidl, C., Pio, C., Puxbaum, H., 2009. Wood burning impact on PM10 in three Austrian regions. Atmos. Environ. 43 (13), 2186–2195.

Cheng, Z., Luo, L., Wang, Y., Wang, Y., Sharma, S., Shimadera, H., Wang, X., Bressi, M., de Miranda, R., Jiang, J., Zhou, W., Fajardo, O., Yan, N., Hao, J., 2016. Status and characteristics of ambient PM2.5 pollution in global megacities. Environ. Int. 89–90, 212–221.

China Data Lab, 2020, "Baidu Mobility Data", https://doi.org/10.7910/DVN/FAEZIO.

Clapp, L.J., Jenkin, M.E., 2001. Analysis of the relationship between ambient levels of O3, NO2 and NO as a function of NOx in the UK. Atmos. Environ. 35, 6391–6405.

C40.org. 2021. C40. [online] Available at: <https://www.c40.org/cities> [Accessed 28 March 2021].

CREA, 2021. [online] Available at: <https://energyandcleanair.org/wp/wp-content/uploads/2020/05/China-air-pollution-rebound-final.pdf> [Accessed 31 March 2021].

Cooper, O., Parrish, D., Ziemke, J., Balashov, N., Cupeiro, M., Galbally, I., Gilge, S., Horowitz, L., Jensen, N., Lamarque, J., Naik, V., Oltmans, S., Schwab, J., Shindell, D., Thompson, A., Thouret, V., Wang, Y. and Zbinden, R., 2014. Global distribution and trends of tropospheric ozone: An observation-based review. Elementa: Science of the Anthropocene, 2.

Dantas, G., Siciliano, B., França, B., da Silva, C., Arbilla, G., 2020. The impact of COVID-19 partial lockdown on the air quality of the city of Rio de Janeiro Brazil. Science of the Total Environment 729, 139085.

Department of Environmental Affairs and Tourism (DEAT), No. 28732 Government Gazette, 21 April 2006, [online] Available at: <https://www.gov.za/sites/default/files/gcis_document/201409/28732b.pdf> [Accessed 28 March 2021].

Deroubaix, A., Brasseur, G., Gaubert, B., Labuhn, I., Menut, L., Siour, G., Tuccella, P., 2020. Response of surface ozone concentration to emission reduction and

meteorology during the COVID-19 lockdown in Europe. Authorea. https://doi.org/10.22541/au.160513378.82834373/v1.

Dhaka, S., Chetna, Kumar, V., Panwar, V., Dimri, A., Singh, N., Patra, P., Matsumi, Y., Takigawa, M., Nakayama, T., Yamaji, K., Kajino, M., Misra, P. and Hayashida, S., 2020. PM2.5 diminution and haze events over Delhi during the COVID-19 lockdown period: an interplay between the baseline pollution and meteorology. Scientific Reports, 10(1), 13442.

EC 2021. Report from the Commission to the European Parliament, The Council, The European Economic and Social Committee and The Committee of the Regions, The Second Clean Air Outlook, European Commission COM(2021) 3 final.

EEA 2020. Air quality in Europe — 2020 report, Luxembourg: Publications Office of the European Union, 2020, ISBN 978-92-9480-292-7, ISSN 1977-8449, doi: 10.2800/786656.

Fang, K., Yao, Q., Guo, Z., Zheng, B., Du, J., Qi, F., Yan, P., Li, J., Ou, T., Liu, J., He, M., Trouet, V., 2021. ENSO modulates wildfire activity in China. Nat. Commun. 12 (1) https://doi.org/10.1038/s41467-021-21988-6.

Fuller, G., Tremper, A., Baker, T., Yttri, K., Butterfield, D., 2014. Contribution of wood burning to PM10 in London. Atmos. Environ. 87, 87–94.

Gama, C., Relvas, H., Lopes, M., Monteiro, A., 2021. The impact of COVID-19 on air quality levels in Portugal: A way to assess traffic contribution. Environ. Res. 193, 110515.

Govender, K., Sivakumar, V., 2019. A decadal analysis of particulate matter (PM2.5) and surface ozone (O3) over Vaal Priority Area South Africa. Clean Air Journal 29, No 2. https://doi.org/10.17159/caj/2019/29/2.7578.

Grange, S., Lee, J., Drysdale, W., Lewis, A., Hueglin, C., Emmenegger, L., Carslaw, D., 2021. COVID-19 lockdowns highlight a risk of increasing ozone pollution in European urban areas. Atmos. Chem. Phys. 21 (5), 4169–4185.

García-Franco, J., 2020. Air quality in Mexico City during the fuel shortage of January 2019. Atmos. Environ. 222, 117131.

Guevara, M., Jorba, O., Soret, A., Petetin, H., Bowdalo, D., Serradell, K., Tena, C., Denier van der Gon, H., Kuenen, J., Peuch, V., Pérez García-Pando, C., 2021. Time-resolved emission reductions for atmospheric chemistry modelling in Europe during the COVID-19 lockdowns. Atmos. Chem. Phys. 21 (2), 773–797.

Gkatzelis, G.I., Gilman, J.B., Brown, S.S., Eskes, H., Gomes, A.R., Lange, A.C., McDonald, B.C., Peischl, J., Petzold, A., Thompson, C.R., Kiendler-Scharr, A., 2021. The global impacts of COVID-19 lockdowns on urban air pollution: A critical review and recommendations. Elem Sci Anth 9 (1), 1–46.

Habibi, H., Awal, R., Fares, A., Ghahremannejad, M., 2020. COVID-19 and the improvement of the global air quality: the bright side of a pandemic. Atmosphere 11 (12), 1279.

Hammer, M.S., van Donkelaar, A., Li, C., Lyapustin, A., Sayer, A.M., Hsu, N.C., Levy, R. C., Garay, M.J., Kalashnikova, O.V., Kahn, R.A., Brauer, M., 2020. Global estimates and long-term trends of fine particulate matter concentrations (1998–2018). Environ. Sci. Technol. 54 (13), 7879–7890.

He, C., Hong, S., Zhang, L., Mu, H., Xin, A., Zhou, Y., Liu, J., Liu, N., Su, Y., Tian, Y., Ke, B., Wang, Y., Yang, L., 2021. Global, continental, and national variation in PM2.5, O3, and NO2 concentrations during the early 2020 COVID-19 lockdown. Atmospheric Pollution Research 12 (3), 136–145.

Hersbach, H., Bell, B., Berrisford, P., Hirahara, S., Horányi, A., Muñoz-Sabater, J., Nicolas, J., Peubey, C., Radu, R., Schepers, D., Simmons, A., Soci, C., Abdalla, S., Abellan, X., Balsamo, G., Bechtold, P., Biavati, G., Bidlot, J., Bonavita, M., Chiara, G., Dahlgren, P., Dee, D., Diamantakis, M., Dragani, R., Flemming, J., Forbes, R., Fuentes, M., Geer, A., Haimberger, L., Healy, S., Hogan, R., Hólm, E., Janisková, M., Keeley, S., Laloyaux, P., Lopez, P., Lupu, C., Radnoti, G., Rosnay, P., Rozum, I., Vamborg, F., Villaume, S., Thépaut, J., 2020. The ERA5 global reanalysis. Q. J. R. Meteorolog. Soc. 146 (730), 1999–2049.

Holloway, T., Levy, H., Kasibhatla, P., 2000. Global distribution of carbon monoxide. J. Geophys. Res.: Atmos. 105 (D10), 12123–12147.

Holzworth, G., 1969. Large-scale weather influences on community air pollution potential in the United States. J. Air Pollut. Control Assoc. 19 (4), 248–254.

Hu, X., Klein, P., Xue, M., Zhang, F., Doughty, D., Forkel, R., Joseph, E., Fuentes, J., 2013. Impact of the vertical mixing induced by low-level jets on boundary layer ozone concentration. Atmos. Environ. 70, 123–130.

Inness, A., Benedetti, A., Flemming, J., Huijnen, V., Kaiser, J., Parrington, M., Remy, S., 2015. The ENSO signal in atmospheric composition fields: emission-driven versus dynamically induced changes. Atmospheric Chemistry and Physics 15, 9083-9097.

Instituto Nacional de Pesquisas Espaciais (INPE), 2021, [online] Available at: <http://queimadas.dgi.inpe.br/queimadas/portal-static/estatisticas_paises/> [Accessed 17 March 2021].

International Cooperative for Aerosol Prediction - Multi-Model Ensemble (ICAP-MME) data, 2021, [online] Available at: https://usgodae.org/ftp/outgoing/nrl/ICAP-MME/ [Accessed 16 March 2021].

Kalogridis, A., Vratolis, S., Liakakou, E., Gerasopoulos, E., Mihalopoulos, N., Eleftheriadis, K., 2018. Assessment of wood burning versus fossil fuel contribution to wintertime black carbon and carbon monoxide concentrations in Athens, Greece. Atmos. Chem. Phys. 18 (14), 10219–10236.

Karagulian, F., Belis, C.A., Dora, C.F.C., Prüss-Ustün, A.M., Bonjour, S., Adair-Rohani, H., Amann, M., 2015. Contributions to cities' ambient particulate matter (PM): a systematic review of local source contributions at global level. Atmos. Environ. 120, 475–483.

Kavassalis, S., Murphy, J., 2017. Understanding ozone-meteorology correlations: A role for dry deposition. Geophys. Res. Lett. 44 (6), 2922–2931.

Krecl, P., Targino, A., Oukawa, G., Cassino Junior, R., 2020. Drop in urban air pollution from COVID-19 pandemic: policy implications for the megacity of São Paulo. Environ. Pollut. 265, 114883.

Kroll, J., Heald, C., Cappa, C., Farmer, D., Fry, J., Murphy, J., Steiner, A., 2020. The complex chemical effects of COVID-19 shutdowns on air quality. Nat. Chem. 12 (9), 777–779.

Kukkonen, J., Kangas, L., Kauhaniemi, M., Sofiev, M., Aarnio, M., Jaakkola, J., Kousa, A., Karppinen, A., 2018. Modelling of the urban concentrations of PM2.5 on a high resolution for a period of 35 years, for the assessment of lifetime exposure and health effects. Atmos. Chem. Phys. 18 (11), 8041–8064.

Kukkonen, J., López-Aparicio, S., Segersson, D., Geels, C., Kangas, L., Kauhaniemi, M., Maragkidou, A., Jensen, A., Assmuth, T., Karppinen, A., Sofiev, M., Hellén, H., Riikonen, K., Nikmo, J., Kousa, A., Niemi, J., Karvosenoja, N., Santos, G., Sundvor, I., Im, U., Christensen, J., Nielsen, O., Plejdrup, M., Nøjgaard, J., Omstedt, G., Andersson, C., Forsberg, B., Brandt, J., 2020. The influence of residential wood combustion on the concentrations of PM2.5 in four Nordic cities. Atmos. Chem. Phys. 20 (7), 4333–4365.

Kumari, P., Toshniwal, D., 2020. Impact of lockdown on air quality over major cities across the globe during COVID-19 pandemic. Urban Clim. 34, 100719.

Lapatinas, A., 2020. The effect of COVID-19 confinement policies on community mobility trends in the EU, EUR 30258 EN. Publications Office of the European Union, Luxembourg.

Le, T., Wang, Y., Liu, L., Yang, J., Yung, Y., Li, G., Seinfeld, J., 2020. Unexpected air pollution with marked emission reductions during the COVID-19 outbreak in China. Science 369 (6504), 702–706.

Liu, Z., Ciais, P., Deng, Z., Lei, R., Davis, S., Feng, S., Zheng, B., Cui, d., Dou, X., Zhu, B., Guo, R., Ke, P., Sun, T., Lu, C., He, P., Wang, Y., Yue, X., Wang, Y., Lei, Y., Zhou, H., Cai, Z., Wu, Y., Guo, R., Han, T., Xue, J., Boucher, O., Boucher, E., Chevallier, F., Tanaka, K., Wei, Y., Zhong, H., Kang, C., Zhang, N., Chen, B., Xi, F., Liu, M., Bréon, F., Lu, Y., Zhang, Q., Guan, D., Gong, P., Kammen, D., He, K., Schellnhuber, H., 2020. Near-real-time monitoring of global CO2 emissions reveals the effects of the COVID-19 pandemic. Nat. Commun. 11 (1).

Maenhaut, W., Vermeylen, R., Claeys, M., Vercauteren, J., Matheeussen, C., Roekens, E., 2012. Assessment of the contribution from wood burning to the PM10 aerosol in Flanders, Belgium. Sci. Total Environ. 437, 226–236.

Maas, R., Grennfelt, P. (eds), 2016. Towards Cleaner Air. Scientific Assessment Report 2016. EMEP Steering Body and Working Group on Effects of the Convention on Long-Range Transboundary Air Pollution, Oslo. xx+50pp.

Mazzeo, N.A., Venegas, L.E., Choren, H. Analysis of NO, NO, O and NO concentrations measured at a green area of Buenos Aires City during wintertime. Atmospheric Environment, 39(17), pp.3055-3068.

McDuffie, E., Smith, S., O' Rourke, P., Tibrewal, K., Venkataraman, C., Marais, E., Zheng, B., Crippa, M., Brauer, M., Martin, R., 2020. A global anthropogenic emission inventory of atmospheric pollutants from sector- and fuel-specific sources (1970–2017): An application of the Community Emissions Data System (CEDS). 10.5194/essd-2020-103.

Mendez-Espinosa, J.F., Rojas, N.Y., Vargas, J., Pechon, J.E., Belalcazar, B.C., Ramírez, O., 2021. Air quality variations in Northern South America during the COVID-19 lockdown. Sci. Total Environ. 749, 141621.

Menut, L., Bessagnet, B., Siour, G., Mailler, S., Pennel, R., Cholakian, A., 2020. Impact of lockdown measures to combat Covid-19 on air quality over western Europe. Sci. Total Environ. 741, 140426.

Millán, M., 2014. Extreme hydrometeorological events and climate change predictions in Europe. J. Hydrol. 518, 206–224.

Monks, P., Archibald, A., Colette, A., Cooper, O., Coyle, M., Derwent, R., Fowler, D., Granier, C., Law, K., Mills, G., Stevenson, D., Tarasova, O., Thouret, V., von Schneidemesser, E., Sommariva, R., Wild, O., Williams, M., 2015. Tropospheric ozone and its precursors from the urban to the global scale from air quality to short-lived climate forcer. Atmos. Chem. Phys. 15 (15), 8889–8973.

Morales-Solís, K., Ahumada, H., Rojas, J.P., Urdanivia, F.R., Catalán, F., Claramunt, T., Toro, R.A., Manzano, C.A., Leiva-Guzmán, M.A., 2021. The Effect of COVID-19 lockdowns on the air pollution of urban areas of central and Southern Chile. Aerosol Air Qual. Res. 21 (8), 200677. https://doi.org/10.4209/aaqr.200677.

NOAA, 2021: https://origin.cpc.ncep.noaa.gov/products/analysis_monitoring/ensostuff/ONI_v5.php; last visited on 01/07/2021).

OECD Statistics. 2021. [online] Available at: <https://stats.oecd.org/> [Accessed 5 March 2021].

Oke, T., Mills, G., Christen, A., Voogt, J., 2017. Urban Climates, 1st ed. Cambridge University Press.

Ordóñez, C., Garrido-Perez, J., García-Herrera, R., 2020. Early spring near-surface ozone in Europe during the COVID-19 shutdown: Meteorological effects outweigh emission changes. Sci. Total Environ. 747, 141322.

OxCGRT, Oxford COVID-19 Government Response Tracker, 2021. COVID-19 Government Response Tracker. [online] Available at: <https://www.bsg.ox.ac.uk/research/research-projects/covid-19-government-response-tracker> [Accessed 3 April 2021].

Parker, H., Hasheminassab, S., Crounse, J., Roehl, C., Wennberg, P., 2020. Impacts of traffic reductions associated with COVID-19 on Southern California air quality. Geophys. Res. Lett. 47 (23).

Parrish, D., Singh, H., Molina, L., Madronich, S., 2011. Air quality progress in North American megacities: a review. Atmos. Environ. 45 (39), 7015–7025.

Petetin, H., Bowdalo, D., Soret, A., Guevara, M., Jorba, O., Serradell, K., Pérez García-Pando, C., 2020. Meteorology-normalized impact of the COVID-19 lockdown upon NO2 pollution in Spain. Atmos. Chem. Phys. 20 (18), 11119–11141.

Philip, S., Martin, R.V., van Donkelaar, A., Lo, J.W.H., Wang, Y., Chen, D., Zhang, L., Kasibhatla, P.S., Wang, S., Zhang, Q., Lu, Z., 2014. Global chemical composition of ambient fine particulate matter for exposure assessment. Environ. Sci. Technol. 48 (22), 13060–13068.

Pomponi, F., Li, M., Sun, Y., Malik, A., Lenzen, M., Fountas, G., D'Amico, B., Akizu-Gardoki, O., Luque Anguita, M., 2020. A novel method for estimating emissions reductions caused by the restriction of mobility: the case of the COVID-19 pandemic. Environ. Sci. Technol. Lett. 8 (1), 46–52.

Poschl, U., Shiraiwa, M., 2015. Multiphase Chemistry at the atmosphere-biosphere interface influencing climate and public health in the Anthropocene. Chem. Rev. 115 (10), 4440–4475.

Querol, X., Massagué, J., Alastuey, A., Moreno, T., Gangoiti, G., Mantilla, E., Duéguez, J., Escudero, M., Monfort, E., Pérez García-Pando, C., Petetin, H., Jorba, O., Vázquez, V., de la Rosa, J., Campos, A., Muñóz, M., Monge, S., Hervás, M., Javato, R., Cornide, M., 2021. Lessons from the COVID-19 air pollution decrease in Spain: Now what? Sci. Total Environ. 779, 146380.

San-Miguel-Ayanz, J., Durrant, T., Boca, R., Maianti, P., Libertá, G., Artés-Vivancos, T., Oom, D., Branco, A., de Rigo, D., Ferrari, D., Pfeiffer, H., Grecchi, R., Nuijten, D. 2020. Advance EFFIS Report on Forest Fires in Europe, Middle East and North Africa 2019, EUR 30222EN, Publications Office of the European Union, Luxembourg, ISBN 978-92-76-18942-8, doi:10.2760/192469, JRC120692.

Seguel, R., Gallardo, L., Fleming, Z., Landeros, S., 2020. Two decades of ozone standard exceedances in Santiago de Chile. Air Qual. Atmos. Health 13 (5), 593–605.

Sessions, W., Reid, J., Benedetti, A., Colarco, P., da Silva, A., Lu, S., Sekiyama, T., Tanaka, T., Baldasano, J., Basart, S., Brooks, M., Eck, T., Iredell, M., Hansen, J., Jorba, O., Juang, H., Lynch, P., Morcrette, J., Moorthi, S., Mulcahy, J., Pradhan, Y., Razinger, M., Sampson, C., Wang, J., Westphal, D., 2015. Development towards a global operational aerosol consensus: basic climatological characteristics of the International Cooperative for Aerosol Prediction Multi-Model Ensemble (ICAP-MME). Atmos. Chem. Phys. 15 (1), 335–362.

Shi, Z., Song, C., Liu, B., Lu, G., Xu, J., Van Vu, T., Elliott, R., Li, W., Bloss, W., Harrison, R., 2021. Abrupt but smaller than expected changes in surface air quality attributable to COVID-19 lockdowns. Sci. Adv. 7 (3), p.eabd6696.

Sicard, P., De Marco, A., Agathokleous, E., Feng, Z., Xu, X., Paoletti, E., Rodriguez, J., Calatayud, V., 2020. Amplified ozone pollution in cities during the COVID-19 lockdown. Sci. Total Environ. 735, 139542.

Siciliano, B., Carvalho, G., da Silva, C., Arbilla, G., 2020. The Impact of COVID-19 Partial Lockdown on Primary Pollutant Concentrations in the Atmosphere of Rio de Janeiro and São Paulo Megacities (Brazil). Bull. Environ. Contaminat. Toxicol. 105 (1), 2–8.

Singh, V., Singh, S., Biswal, A., Kesarkar, A., Mor, S., Ravindra, K., 2020. Diurnal and temporal changes in air pollution during COVID-19 strict lockdown over different regions of India. Environ. Pollut. 266, 115368.

Singh, V., Singh, S., Biswal, A., 2021. Exceedances and trends of particulate matter (PM2.5) in five Indian megacities. Sci. Total Environ. 750, 141461.

Singh, V., Sokhi, R.S., Kukkonen, J., 2014. PM2. 5 concentrations in London for 2008–A modeling analysis of contributions from road traffic. J. Air Waste Manage. Assoc. 64 (5), 509–518.

Sun, J., Li, H., Zhang, W., Li, T., Zhao, W., Zuo, Z., Guo, S., Wu, D., Fan, S., 2018. Modulation of the ENSO on Winter Aerosol Pollution in the Eastern Region of China. J. Geophys. Res.: Atmos. 123, 11952–11969.

van Heerwaarden, C., Mol, W., Veerman, M., Benedict, I., Heusinkveld, B., Knap, W., Kazadzis, S., Kouremeti, N., Fiedler, S., 2021. Record high solar irradiance in Western Europe during first COVID-19 lockdown largely due to unusual weather. Commun. Earth Environ. 2 (1).

Venter, Z.S., Aunan, K., Chowdhury, S., Lelieveld, J., 2020. COVID-19 lockdowns cause global air pollution declines. PNAS 117 (32), 18984–18990.

Wang, J X.L., Angell, J.K., 1999. Air stagnation climatology for the United States (1948–1998). [online] Osti.gov. Available at: <https://www.osti.gov/biblio/6408773-air-stagnation-climatology-united-states> [Accessed 6 March 2021].

Wang, Y., Wen, Y., Wang, Y., Zhang, S., Zhang, K., Zheng, H., Xing, J., Wu, H., Hao, J., 2020a. Four-month changes in air quality during and after the COVID-19 Lockdown in Six Megacities in China. Environ. Sci. Technol. Lett. 7 (11), 802–808.

Wang, P., Chen, K., Zhu, S., Wang, P., Zhang, H., 2020b. Severe air pollution events not avoided by reduced anthropogenic activities during COVID-19 outbreak. Resour. Conserv. Recycl. 158, 104814.

Wang, S., Du, L., Tsona, N.T., Jiang, X., You, B., Xu, L., Yang, Z., Wang, W., 2020c. Effect of NOx and SO2 on the photooxidation of methylglyoxal: Implications in secondary aerosol formation. J. Environ. Sci. 92, 151–162.

WAQI, 2020. World's Air Pollution Real-time air quality index. https://aqicn.org/data-platform/covid19/verify/.

Wiedinmyer, C., Yokelson, R., Gullett, B., 2014. Global emissions of trace gases, particulate matter, and hazardous air pollutants from open burning of domestic waste. Environ. Sci. Technol. 48 (16), 9523–9530.

World Health Organization, 2006. Air Quality Guidelines. Global Update 2005. [online] Available at: <https://apps.who.int/iris/bitstream/handle/10665/69477/WHO_SDE_PHE_OEH_06.02_eng.pdf> [Accessed 12 April 2021].

World Meteorological Organization, 2021a. First Report of the WMO COVID-19 Task Team: Review on Meteorological and Air Quality Factors Affecting the COVID-19 Pandemic (WMO-No. 1262). Part I: First COVID-19 report. Part II: Executive Summary (multilingual).

World Meteorological Organization. 2021b. Sand and Dust Storm Warning Advisory and Assessment System (Forecast Maps). [online] Available at: <https://public.wmo.int/en/our-mandate/focus-areas/environment/SDS/warnings> [Accessed 6 March 2021].

Yan, Y., Pozzer, A., Ojha, N., Lin, J., Lelieveld, J., 2018. Analysis of European ozone trends in the period 1995–2014. Atmos. Chem. Phys. 18 (8), 5589–5605.

Zambrano-Monserrate, M., Ruano, M., 2020. Has air quality improved in Ecuador during the COVID-19 pandemic? A parametric analysis. Air Qual. Atmos. Health 13 (8), 929–938.

Zhai, S., Jacob, D., Wang, X., Shen, L., Li, K., Zhang, Y., Gui, K., Zhao, T., Liao, H., 2019. Fine particulate matter (PM2.5) trends in China, 2013–2018: separating contributions from anthropogenic emissions and meteorology. Atmos. Chem. Phys. 19(16), 11031-11041.

Zhang, Q., Zheng, Y., Tong, D., Shao, M., Wang, S., Zhang, Y., Xu, X., Wang, J., He, H., Liu, W., Ding, Y., Lei, Y., Li, J., Wang, Z., Zhang, X., Wang, Y., Cheng, J., Liu, Y., Shi, Q., Yan, L., Geng, G., Hong, C., Li, M., Liu, F., Zheng, B., Cao, J., Ding, A., Gao, J., Fu, Q., Huo, J., Liu, B., Liu, Z., Yang, F., He, K. and Hao, J., 2019. Drivers of improved PM2.5 air quality in China from 2013 to 2017. Proc. Natl. Acad. Sci. 116(49), 24463–24469.

Zhao, S., Zhang, H., Xie, B., 2018. The effects of El Niño-Southern Oscillation on the winter haze pollution of China. Atmos. Chem. Phys. 18, 1863–1877.

Zhao, N., Wang, G., Li, G., Lang, J., Zhang, H., 2020. Air pollution episodes during the COVID-19 outbreak in the Beijing–Tianjin–Hebei region of China: An insight into the transport pathways and source distribution. Environ. Pollut. 267, 115617.

Zheng, B., Chevallier, F., Ciais, P., Yin, Y., Deeter, M., Worden, H., Wang, Y., Zhang, Q., He, K., 2018a. Rapid decline in carbon monoxide emissions and export from East Asia between years 2005 and 2016. Environ. Res. Lett. 13 (4), 044007.

Zheng, B., Chevallier, F., Yin, Y., Ciais, P., Fortems-Cheiney, A., Deeter, M., Parker, R., Wang, Y., Worden, H., Zhao, Y., 2019. Global atmospheric carbon monoxide budget 2000–2017 inferred from multi-species atmospheric inversions. Earth Syst. Sci. Data 11 (3), 1411–1436.

Zheng, B., Geng, G., Ciais, P., Davis, S., Martin, R., Meng, J., Wu, N., Chevallier, F., Broquet, G., Boersma, F., van der A, R., Lin, J., Guan, D., Lei, Y., He, K. and Zhang, Q., 2020. Satellite-based estimates of decline and rebound in China's CO2 emissions during COVID-19 pandemic. Sci. Adv. 6(49), p.eabd4998.

Zheng, B., Tong, D., Li, M., Liu, F., Hong, C., Geng, G., Li, H., Li, X., Peng, L., Qi, J., Yan, L., Zhang, Y., Zhao, H., Zheng, Y., He, K., Zhang, Q., 2018b. Trends in China's anthropogenic emissions since 2010 as the consequence of clean air actions. Atmos. Chem. Phys. 18 (19), 14095–14111.

Zhu, W., Xu, X., Zheng, J., Yan, P., Wang, Y., Cai, W., 2018. The characteristics of abnormal wintertime pollution events in the Jing-Jin-Ji region and its relationships with meteorological factors. Sci. Total Environ. 626, 887–898.